



Fine and coarse dust separation with polarization lidar

R. E. Mamouri¹ and A. Ansmann²

¹Cyprus University of Technology, Dep. of Civil Engineering and Geomatics, Limassol, Cyprus

²Leibniz Institute for Tropospheric Research, Leipzig, Germany

Correspondence to: R. E. Mamouri (rodanthi.mamouri@cut.ac.cy)

Received: 21 April 2014 – Published in Atmos. Meas. Tech. Discuss.: 23 May 2014

Revised: 14 September 2014 – Accepted: 22 September 2014 – Published: 10 November 2014

Abstract. The polarization-lidar photometer networking (POLIPHON) method for separating dust and non-dust aerosol backscatter and extinction, volume, and mass concentration is extended to allow for a height-resolved separation of fine-mode and coarse-mode dust properties in addition. The method is applied to a period with complex aerosol layering of fine-mode background dust from Turkey and Arabian desert dust from Syria. The observation was performed at the combined European Aerosol Research Lidar Network (EARLINET) and Aerosol Robotic Network (AERONET) site of Limassol (34.7° N, 33° E), Cyprus, in September 2011. The dust profiling methodology and case studies are presented. Consistency between the column-integrated optical properties obtained with sun/sky photometer and the respective results derived by means of the new lidar-based method corroborate the applicability of the extended POLIPHON version.

1 Introduction

Mineral dust is a major component of the atmospheric aerosol system, uniquely influencing climatic and environmental conditions. The deserts in northern Africa and in the Middle East (western Asia) are major dust sources and have a strong impact on air quality and aerosol conditions in southern and eastern Europe. Large amounts of mineral dust can be advected over long distances in the lower free troposphere from these deserts to remote areas within a few days (Ansmann et al., 2003; Papayannis et al., 2008; Baars et al., 2011). Turbulent exchange processes at the interface between the free troposphere and the planetary boundary layer lead to efficient downward mixing of dust towards the surface. Emissions from arid (non-desert) and semi-arid regions and areas

with strong agricultural activities also contribute to the dust load over Europe.

For a proper consideration of mineral dust in climate modeling and air quality monitoring efforts, vertical profiling of dust with the potential to distinguish between fine-mode and coarse-mode dust is required (Kok, 2011; Zhang et al., 2013). The fine mode covers by definition the particle size spectrum up to 1 μm in diameter, whereas the coarse mode contains the supermicrometer dust particles (diameters greater than 1 μm). Fine and coarse dust particles influence the Earth's radiation budget, cloud processes, and environmental conditions in different ways (Nabat et al., 2012; Mahowald et al., 2014). The optical properties and radiative impact are widely controlled by coarse-mode dust particles. However, 20–40 % of the dust-related optical depth is caused by fine-mode dust according to Aerosol Robotic Network (AERONET) sun/sky photometer observations (see Sect. 3). Regarding the influence on cloud processes, coarse dust particles belong to the most favorable cloud condensation and ice nuclei (DeMott et al., 2010). Fine-mode dust particles, on the other hand, can significantly impact air quality, defined in PM (particulate matter) aerosol levels, and may even sometimes dominate PM_{1.0} (particles with diameters less than 1.0 μm) observations at sites close to deserts, such as Cyprus. As an example, on 1 April 2013, the 500 nm aerosol particle optical thickness (AOT) increased from 1 to 4 between 08:00 and 12:00 UTC over Cyprus during a rather strong Saharan dust outbreak. These large AOT values indicate fine-mode dust mass concentrations of 35–140 $\mu\text{g m}^{-3}$ in the tropospheric column up to 4–5 km in height, which is 10–15 % of the total dust mass concentration.

In this contribution, we present the first attempt to use empirical knowledge on the light-depolarizing properties of fine-mode and coarse-mode dust (Sakai et al., 2010) in the

interpretation of polarization lidar observations, with the goal of separating fine-mode, coarse-mode, and remaining non-dust aerosol components. To date, polarization lidars have been used to identify dust and to separate backscatter and extinction coefficients of dust and non-dust aerosol (e.g., Sugimoto and Lee, 2006; Nishizawa et al., 2007; Tesche et al., 2009, 2011; Groß et al., 2011; Ansmann et al., 2011a, 2012). The most important parameter in these studies is the so-called particle linear depolarization ratio (frequently simply denoted as the depolarization ratio).

Our attempt to develop a method for fine and coarse dust separation, as an extension of the Polarization Lidar Photometer Networking (POLIPHON) method (Ansmann et al., 2012), was motivated by observations of enhanced free-tropospheric depolarization ratios of 10–20% with the European Aerosol Research Lidar Network (EARLINET) polarization lidar over Limassol (34.7° N, 33° E, 50 m above sea level, a.s.l.), Cyprus. Such values indicate the presence of dust. At the same time, however, AERONET sun/sky photometer measurements indicated the absence of coarse-mode dust particles. These enhanced depolarization ratios were thus most likely exclusively caused by fine-mode dust particles. According to laboratory studies of Sakai et al. (2010) for a laser wavelength of 532 nm, dust particle size distributions dominated by fine-mode particles cause particle depolarization ratios of around 0.16 ± 0.05 , whereas particle depolarization ratios of 0.39 ± 0.04 were observed in the presence of a high number of desert dust particles in the supermicrometer range (coarse-mode particles). The laboratory studies are discussed further in Sect. 4.

Presently, several new dust profiling methods are being tested, built on existing AERONET and EARLINET measurements in Europe. Two fundamentally different lidar-/photometer-based retrieval concepts are applied. On the one hand, the Lidar/Radiometer Inversion Code (LIRIC) (Chaikovskiy et al., 2012) and the Generalized Aerosol Retrieval from Radiometer and Lidar Combined data (GARRLiC) methods (Lopatin et al., 2013) are used. As an alternative technique, the POLIPHON approach (Ansmann et al., 2012) was developed.

LIRIC uses profiles of elastic-backscatter lidar return signals at 355, 532, and 1064 nm and, as a priori assumptions, AERONET retrieval products (column-integrated particle size distribution, composition, complex refractive index) based on a particle shape model. The irregularly shaped dust particles are assumed to be spheroidal dust particles. This approach works well in the case of the analysis of pure sun/sky photometer data (Dubovik et al., 2006). However, it is shown by Wagner et al. (2013) that this particle shape model introduces significant uncertainties in the LIRIC aerosol products when applied to lidar backscatter returns (i.e., to light scattering information for a scattering angle of exactly 180°). Products of the LIRIC data analysis are height profiles of particle backscatter and extinction coefficients at the three wavelengths, and particle volume and mass

concentration profiles separately for fine-mode and coarse-mode spherical particles and coarse-mode non-spherical particles.

GARRLiC is an extended version of LIRIC, and pursues an even deeper synergy of lidar and radiometer data in the retrievals. To apply the LIRIC and GARRLiC methods, lidar and photometer observation have to be performed simultaneously. Thus, cloudfree conditions are required.

In contrast, the POLIPHON approach is designed explicitly to avoid the use of a particle shape model and also a strong dependence on photometer observations. POLIPHON is applicable even in cloudy conditions, which often occur during dust outbreaks, and thus is able to be applied in aerosol–cloud interaction studies. The technique is based on measured 180° light-depolarization characteristics for dust aerosol particles.

This approach was originally developed for the separation of non-dust (spherical fine-mode) and dust (non-spherical coarse-mode) particle backscatter coefficients. The data analysis is straightforward and performed in one computational step. We denote this approach therefore as the one-step POLIPHON method in the following. The extended POLIPHON formalism allows the separation of non-dust, fine, and coarse dust particle backscatter coefficients. The data analysis is performed in two computational steps (the two-step POLIPHON method). Both methods for the retrieval of optical properties, volume, and mass concentrations are outlined in Sect. 5. POLIPHON belongs to the family of well-established lidar aerosol-typing methods that built on empirically gathered optical aerosol properties as presented by Groß et al. (2013) and Burton et al. (2014).

In Sect. 2, the lidar and photometer instruments are briefly described. Section 3 presents an overview of typical optical properties of desert dust in terms of fine-mode and coarse-mode dust optical depth, the fine-mode optical depth fraction, and Ångström exponents. This section is presented to emphasize the need for the development of more sophisticated fine and coarse dust separation techniques. In Sect. 4, an overview of relevant light-depolarizing aerosol types is given, including their characteristic particle linear depolarization ratios. This section also discusses the potential impact (interference) of non-dust, but sensitively depolarizing aerosol components in biasing our dust profiling efforts. After the presentation of the one-step and two-step POLIPHON methodologies in Sect. 5, the new dust retrieval scheme is then applied to an episode with complex aerosol layering with background fine-mode dust as well as desert dust (coarse and fine dust) during a strong dust outbreak in September 2011 (Sect. 6). Summarizing and concluding remarks are given in Sect. 7.

2 Instrumentation

2.1 Polarization lidar

The lidar station of the Cyprus University of Technology (CUT) at Limassol is located about 150 km south of Turkey and 250 km west of Syria (Mamouri et al., 2013). The source laser transmits linear-polarized pulses, and the receiving unit detects the parallel- and cross-polarized signal components with respect to the plane of laser polarization at a 532 nm wavelength. The ratio of the calibrated cross-polarized to parallel-polarized signal yields the volume linear depolarization ratio from which the particle depolarization ratio can be computed (e.g., Tesche et al., 2009). The lidar has four channels for the measurement of the parallel- and cross-polarized signal components at 532 nm, the total backscatter signal at 1064 nm, and the nitrogen Raman backscatter signal at 607 nm. Calibration of the polarization channels is performed by rotating the box with the polarization-sensitive channels following the methodology of Freudenthaler et al. (2009). The transmission properties of the receiver (for parallel and perpendicularly polarized light) required for an accurate determination of the particle linear depolarization ratio are available from test and calibration measurements.

The full overlap of the laser beam with the receiver field of view of the 20 cm Cassegrain telescope is obtained at heights around 300 m a.s.l. The overlap characteristics were checked by Raman lidar observations at 532 and 607 nm (Wandinger and Ansmann, 2002) under clear sky conditions at Limassol. The measured volume depolarization ratio is reliable to about 50 m above the ground. Overlap effects widely cancel each other out here because the depolarization ratio is calculated from the ratio of the cross-polarized to the parallel-polarized signal component (Freudenthaler et al., 2009).

In this paper, we will make use of the particle backscatter coefficient and the particle depolarization ratio at 532 nm. The determination of the particle backscatter coefficient is described by Mamouri et al. (2013). For the calibration of the profile of the measured 532 nm elastic backscatter signal, pure Rayleigh signals are simulated based on actual temperature and pressure profiles from numerical weather forecast data or actual nearby radiosonde observations. The measured 532 nm signals are then fitted to the Rayleigh signal profile in the aerosol-free middle to upper troposphere. The corresponding reference particle backscatter coefficient was set to zero at heights above 4–5 km in the particle backscatter retrieval, after Sasano et al. (1985). The particle depolarization ratio is computed from the volume depolarization ratio by means of the determined particle backscatter coefficient (Freudenthaler et al., 2009). Uncertainties in the retrieval products are discussed by Mamouri et al. (2013), and are typically on the order of 5–10 %.

For the lowermost heights (below 300 m, where the overlap between the laser beam and the receiver field-of-view is incomplete), we assumed a linear decrease by roughly

a factor of 2 in particle backscattering from the surface (strongly influenced by Limassol urban haze) to 300 m in height (Mamouri et al., 2013). This assumption about the lowermost part of the backscatter profile is based on careful inspections of night aerosol Raman observations, i.e., of the profiles of the signal ratio of the 532 nm elastic backscatter signal to the 607 nm nitrogen Raman signal. This signal ratio is essentially independent of the overlap effect. The impact of the lowermost 300 m on our retrieval products and the subsequent comparisons with AERONET photometer column data is low (the AOT contribution is on the order of 10 %) in the case of the discussed desert dust outbreak observations.

2.2 Sun/sky photometer

The lidar is collocated with a sun/sky photometer of the Aerosol Robotic Network (AERONET, CUT-TEPAK site, Limassol, Cyprus, <http://aeronet.gsfc.nasa.gov>) (Holben et al., 1998). The CUT-AERONET photometer allows the retrieval of the aerosol optical thickness (AOT) at eight wavelengths from 339 to 1638 nm. Sky radiance observations at four wavelengths complete the AERONET observations. From the spectral AOT distribution, the Ångström exponent AE (Ångström, 1964) and the fine-mode fraction FMF (fraction of fine-mode AOT to total AOT) (O'Neill et al., 2003b) are obtained. By including sky radiance observations in the data analysis, the volume size distribution of the particles and the fine-mode volume fraction FVF (fraction of fine-mode volume concentration to total particle volume concentration) can be retrieved.

AOT errors are on the order of 0.01–0.02 in the absence of unfiltered cloud contamination (Chew et al., 2012). Undefined uncertainties can occur in the AERONET retrieval of the volume size distribution and FVF close to desert dust sources, where a considerable number of dust particles with radii greater than 15 μm may be present and influence the measured optical properties (Müller et al., 2010). The AERONET inversion algorithm used to derive the particle size distribution only considers particles with radii less than 15 μm .

3 Fine- and coarse-mode optical properties of mineral dust observed with AERONET photometers

Before presenting the new two-step POLIPHON approach, we want to discuss the fine-mode dust impact on overall dust optical and microphysical properties, and to provide convincing arguments that the development of lidar methods allowing discrimination of fine and coarse dust profiles is useful and important for atmospheric and environmental research.

The first example, shown in Fig. 1, is a major Saharan dust outbreak reaching Cyprus on 1 April 2013. According to Fig. 2, the 500 nm AOT increased from 1 to 4 within 4 hours (08:00–12:00 UTC) over Limassol. Disregarding the

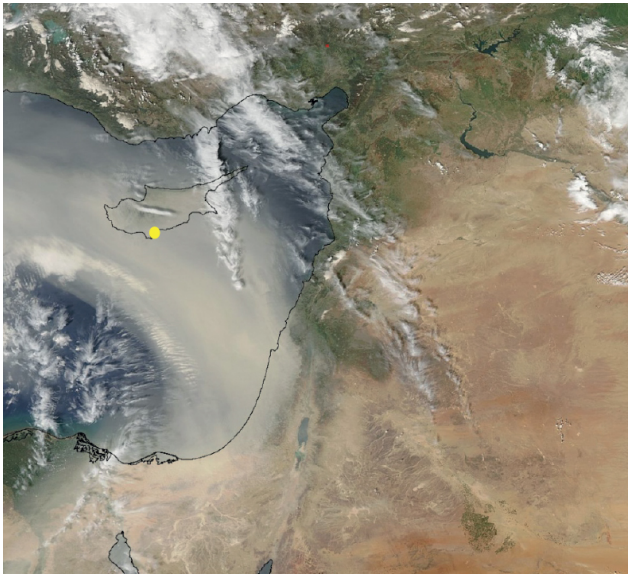


Figure 1. Major Saharan dust outbreak moving northward and striking Cyprus on 1 April 2013 (AQUA–MODIS image, 10:40 UTC). The yellow circle indicates the combined EARLINET–AERONET station of Limassol.

rather strong AOT increase, the fine-mode fraction remained almost constant. About 25 % of the 500 nm AOT was caused by fine-mode dust. As mentioned, fine-mode particles are those particles with radii ≤ 500 nm. However, in accordance with AERONET observations, particles with radii < 300 nm are mainly responsible for the observed fine-mode 500 nm AOT (O'Neill et al., 2003a).

Figure 3 gives an overview of the dust observations from AERONET during the Saharan Mineral Dust Experiment 1 (SAMUM-1) (Heintzenberg, 2009; Ansmann et al., 2011b), including 500 nm AOT, AE, FMF, and FVF. The SAMUM-1 field site of Ouarzazate (30.9° N, 6.9° W, 1150 m a.s.l.), Morocco, is very close to the Sahara, with a minimum impact of non-dust aerosol components on the photometer observations. Two pronounced dust outbreaks from Algeria are indicated in Fig. 3. FMF ranges from 0.2 to 0.4 during these strong dust events. Figure 4 shows two dust particle size distributions measured within the two SAMUM-1 dust outbreak periods. During these specific periods, the FMF values are 0.24–0.35, and again indicate a significant influence of fine-mode dust on the measured optical properties. The fine-mode volume fraction ranges from 10 to 15 %. These two observational cases corroborate the finding that a lidar-based separation of fine and coarse dust profiles in terms of optical and microphysical properties is a useful addition to atmospheric profiling techniques.

In the discussion and interpretation of our observations in Sect. 5, we need characteristic values for the dust Ångström exponent, separately for fine mode and coarse mode. As can be seen from Figs. 3 and 4, fine-mode dust AE is about

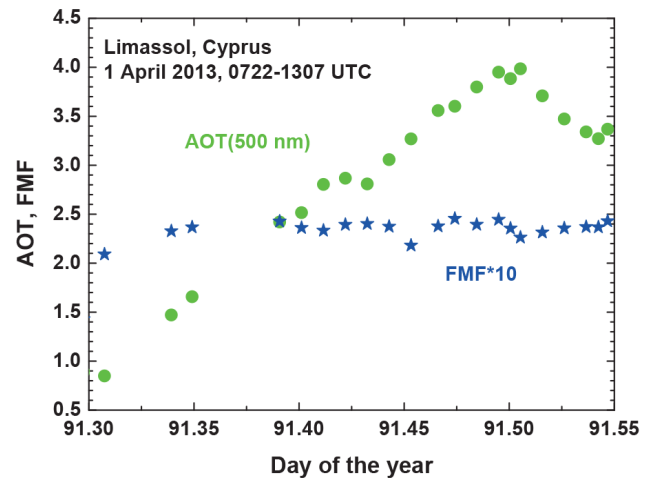


Figure 2. 500 nm aerosol particle optical thickness (AOT, green circles) and fine-mode fraction (FMF multiplied by a factor of 10, blue stars), observed with the AERONET sun/sky photometer on 1 April 2013. Peak AOT values reached 4.0 around noon. The dust-dominated FMF was always close to 0.24.

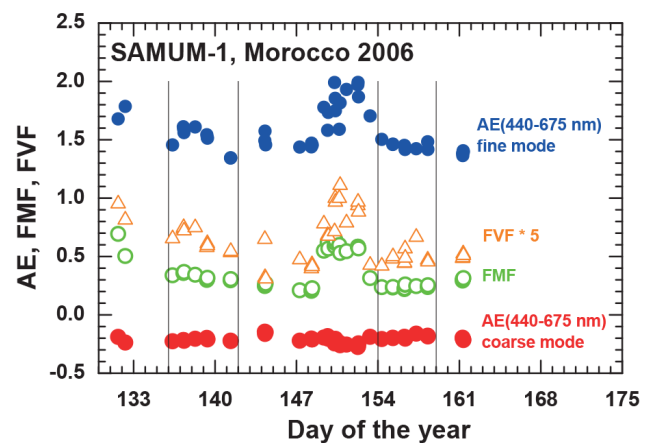


Figure 3. SAMUM-1 pure Saharan dust Ångström exponent AE (440–675 nm) for fine mode (blue circles) and coarse mode (red circles), fine-mode 500 nm AOT fraction FMF (open green circles), and fine-mode particle volume fraction FVF (multiplied by a factor of 5, open orange triangles) observed with the AERONET sun/sky photometer. The measurements were performed at Ouarzazate (30.9° N, 6.9° W), very close to the Sahara in southeastern Morocco. Pure dust episodes occurred from 136 to 142 (16–21 May 2006) and from 154 to 159 (3–7 June 2006, indicated by vertical lines).

1.5 ± 0.1 , and coarse-mode AE is close to -0.2 ± 0.05 . In addition, we need particle extinction-to-volume conversion factors to translate lidar-derived profiles of the dust extinction coefficient into volume and mass concentrations. In Fig. 4, these conversion factors (v_f / AOT_f , v_c / AOT_c) are computed from the retrieved AERONET values of column-integrated particle volume concentrations (v_f , v_c) for

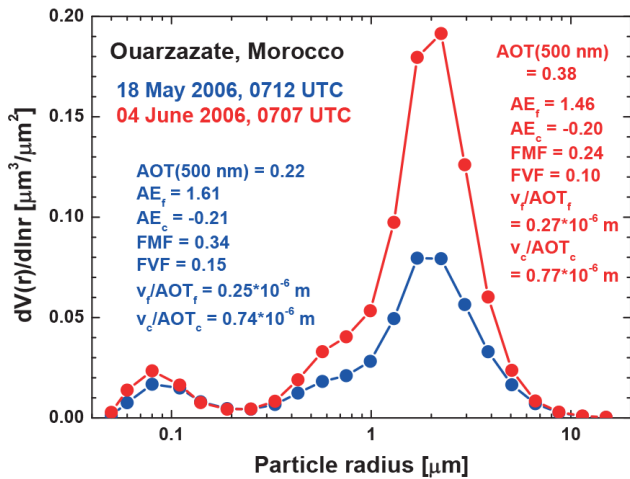


Figure 4. Column-integrated particle volume concentration as a function of particle radius (22 radius intervals) of pure Saharan dust observed with the AERONET photometer over Ouarzazate, southern Morocco, during SAMUM-1 on the morning of 18 May 2006 (blue) and 4 June 2006 (red). Values for 500 nm AOT, fine-mode and coarse-mode Ångström exponents AE_f and AE_c , fine-mode fraction FMF, and fine-mode particle volume fraction FVF are given in addition. Conversion factors v_f/AOT_f and v_c/AOT_c for fine-mode and coarse-mode dust with volume concentrations v_f and v_c , respectively, are needed in the conversion of the lidar-derived optical properties into volume and mass concentrations by means of the POLIPHON method (see Sect. 5).

fine-mode and coarse-mode dust, respectively, and corresponding particle optical depths (500 nm AOT_f , AOT_c). The SAMUM-1 conversion factors in Fig. 4 are in good agreement with simulations of Barnaba and Gobbi (2004). Based on several thousands of realistic combinations of particle number concentration, size distribution, and refractive index characteristics, the volume-to-extinction ratio v_{dc}/τ_{dc} for dust size distributions dominated by supermicrometer dust particles typically ranges from 0.6 to 0.9×10^{-6} m for 532 nm wavelength. τ_{dc} indicates the coarse-mode dust optical thickness in the equations in Sect. 5. The maximum value is 1.0×10^{-6} m for very large dust particles. For submicrometer-dust-dominated particle ensembles, the conversion factor v_{df}/τ_{df} is between 0.25×10^{-6} m and 0.4×10^{-6} m. For non-dust, fine-mode-dominated size distributions (representing anthropogenic pollution), the conversion factor v_{nd}/τ_{nd} is around 0.18×10^{-6} m. An extended discussion of the range of observed conversion factors is given by Ansmann et al. (2012).

4 Light depolarization by atmospheric aerosols and potential bias of dust profiling by non-dust aerosol

By using the polarization lidar technique for quantitative dust profiling, a good knowledge of the light-depolarization

characteristics (for 180° scattering) of a variety of aerosol types is necessary (see Sect. 4.1). In addition, a careful aerosol source identification (backward trajectory analysis) for the time period of the lidar measurement is required to check the potential interference (bias) of dust profiling by light depolarization by other aerosol components that are able to disturb dust detection considerably (see Sect. 4.2). Lidar observations should also be compared with sun/sky photometer measurements for consistency, which enhances the reliability of the lidar products (see Sect. 5.3).

4.1 Depolarization ratio of different aerosol types

Sakai et al. (2010) investigated the depolarization characteristics of Asian and Saharan dust probes at 532 nm in laboratory studies. For the linear depolarization ratio for size distributions dominated by submicrometer dust particles (i.e. fine-mode dust), particle linear depolarization ratios of $17 \pm 2\%$ (Asian dust) and $14 \pm 3\%$ (Saharan dust) were found. The different mean values for Asian and Saharan dust may result from the variable, not well-defined amount of remaining supermicrometer dust particles in the used submicrometer dust probes, and not from differences in the shape characteristics. In Sect. 4, we use $\delta_{df} = 16\%$ as a characteristic fine-mode dust depolarization ratio. For size distributions, dominated by supermicrometer dust particles, Sakai et al. (2010) determined particle depolarization ratios of $39 \pm 5\%$ for both Asian and Saharan dust. Consequently, we use $\delta_{dc} = 39\%$ as a characteristic coarse-mode dust depolarization ratio in the derivations presented in Sect. 5.

As stated above, the fine-mode 500 nm AOT (and thus backscatter and extinction) is mainly caused by scattering and absorption by particles with a radius of less than 300 nm (O'Neill et al., 2003a). For the respective lognormal particle size distributions, J. Gasteiger (personal communication, 2014) obtains linear particle depolarization ratios of around $15 \pm 5\%$ from simulations with a variety of models of irregularly shaped dust particles as presented in Gasteiger et al. (2011). For lognormal size distributions dominated by coarse supermicrometer dust particles, the simulations yield values of around $40 \pm 5\%$ (J. Gasteiger, personal communication, 2014). All these simulated values are thus in good agreement with the laboratory studies of Sakai et al. (2010).

These findings of Sakai et al. (2010) are also consistent with the field observations close to the Sahara (Freudenthaler et al., 2009; Groß et al., 2011). In these field studies, the pure dust depolarization ratio ranged from 30 to 35% at 532 nm, with a mean value of $\delta_d = 31 \pm 3\%$. These values can be reproduced with fine and coarse dust depolarization ratios of 16 and 39% when assuming a fine-mode contribution to the total dust particle backscatter coefficient of about 25%. Particle depolarization ratios of 30–35% are also observed in cases of Asian desert dust (Sugimoto et al., 2003; Shimizu et al., 2004) and desert dust from Middle East dust sources

(Mamouri et al., 2013). In our POLIPHON method, we use $\delta_d = 31\%$ as the overall dust depolarization ratio.

However, despite the good agreement between the model and laboratory studies, many more investigations are required to obtain a robust and trustworthy basis on fine-mode and coarse-mode dust depolarization ratios for our new approach to separate fine and coarse dust particles. There is still room to test a variety of dust shape models. Laboratory and simulation studies should cover the laser wavelengths of 355, 532, and 1064 nm. We are convinced that mineral dust, released into the atmosphere, has characteristic (universal) shape properties, and that these properties do not vary from dust source to dust source. Otherwise it would be not understandable why pure dust plumes produce almost everywhere (e.g., in eastern Asia, for Middle East dust, Saharan dust) similar particle depolarization ratios of 30–35%. This may facilitate the simulations studies towards the identification of the most realistic dust shape characteristics. Furthermore, if the brittle fragmentation theory (Kok, 2011) correctly describes the size distribution of dust released into the atmosphere over deserts by wind stress and subsequent atmospheric removal processes have the same impact on dust size distributions of long-range-transported dust all over the world (Nabat et al., 2012) then there should also be a characteristic size distribution of desert dust particles (the usually observed bimodal size distribution). This may further facilitate simulation efforts and comparison with lidar field observations.

Regarding observable dust size distributions and the related optical properties, it should be mentioned that the assumptions about the fine/coarse dust fractions (as shown in Sect. 3 for desert dust outbreaks) are less clear for soil dust injected into the atmosphere during fire events (Nisantzi et al., 2014). The role of the rather hot air close to the ground in dust release and the resulting dust size distribution is not well known. Wind stress close to the ground may be very complex, and the sudden release of all the moisture in the heated soil particles may strongly influence the cracking of larger particles into smaller ones, and thus may lead to a much more complicated size distribution than observed during desert dust outbreaks. In addition, observations of Dahlkötter et al. (2014) and other studies (compiled and discussed in that publication) show that the dust fraction in aged fire smoke plumes is dominated by fine-mode dust. The coarse particles are widely removed. Such features (i.e., fine dust only) are not observed during desert dust outbreaks, as the AERONET observations and our experience from field studies such as SAMUM and the Saharan Aerosol Long-range Transport and Aerosol-Cloud interaction Experiment (SALTRACE) (Ansmann et al., 2014) clearly show.

Concerning the depolarization features of other potentially light-depolarizing aerosol types, we assume that wet marine particles produce a depolarization ratio of close to 2–3% (Groß et al., 2011, 2013). From recent SALTRACE observations at Barbados in February 2014 under rather clean

free-tropospheric conditions, with relative-humidity changes from 80% at the top of the boundary layer to 5% about 200 m higher up, we conclude that the impact of dry marine particles (sea salt particles) on depolarization ratio measurements must be generally weak. We observed enhanced depolarization ratios of about 4–6% at 532 and 1064 nm in the entrainment zone (in the mixture of wet and dry marine particles) and no impact of marine particles on the lidar measurements higher up in the free troposphere. We expected much higher depolarization values caused by dry cubic-like sea salt particles at 5% ambient relative humidity. The laboratory studies of Sakai et al. (2010) revealed that dry sea salt particles may cause depolarization ratios of up to about 10%. This is roughly in agreement with simulations by J. Gasteiger (personal communication, 2014), who found increases in the depolarization ratio from 2% for wet spherical sea salt particles to 10–15% for dry particles with a cubic shape.

Further light-depolarizing aerosol components are pollen, for which depolarization ratios are unknown (Noh et al., 2013), and volcanic ash particles (Ansmann et al., 2010; Groß et al., 2012). Large pollen particles (of up to 50 μm in diameter and more) may cause depolarization ratios as large as the ones for desert and volcanic dust particles. Volcanic dust particles cause depolarization ratios between 30 and 40%.

4.2 Interference of dust profiling by depolarizing non-dust aerosol components

As a result of our long-term lidar observations in marine environments since 1997, we assume that dry marine particles play a negligible role in atmospheric polarization lidar studies of dust. Marine particles are always wet in the boundary layer at the generally high relative humidities around 70–90%. The amount of dry marine particles in the free troposphere is expected to be always rather low.

Volcanic particles may introduce large uncertainties in desert or soil dust retrieval with polarization lidars, but their influence can be neglected in volcanically quiescent times. Furthermore, backward trajectory analysis helps to identify a potential bias by volcanic aerosols.

The remaining light-depolarizing component is biogenic pollen aerosol. However, as Noh et al. (2013) reported, a considerable impact of pollen particles with observed enhanced total particle depolarization ratios of up to 15% in the boundary layer occurred only during daytime hours, when the boundary layer convection is strong, and this only during the spring season. The impact was not visible in the free troposphere.

All in all, interference of desert and soil dust profiling by other light-depolarizing particles can be regarded as weak. The non-dust-related depolarization ratio δ_{nd} may vary from 1.5 to 15%, according to the literature. The values accumulate around 5%, according to published values (Murayama

et al., 1999, 2004; Fiebig et al., 2002; Sugimoto et al., 2003; Müller et al., 2005, 2007; Sugimoto and Lee, 2006; Chen et al., 2007; Heese and Wiegner, 2008). By assuming a depolarization ratio of $\delta_{nd} = 5\%$ for the overall non-dust effect on light depolarization in our method presented in Sect. 4, we consider all contributions of traces of dried marine particles, of pollen aerosol, and potential traces of volcanic ash in our lidar data analysis. In summary, we assume that fine and coarse dust particles are the only significant depolarizing atmospheric aerosol components that have to be considered in our polarization lidar retrieval.

5 Extended POLIPHON method

The new two-step POLIPHON method uses the same separation technique as the one-step approach. The latter method is described in detail by Tesche et al. (2009) for a two-aerosol component mixture of desert dust and biomass burning smoke. We briefly introduce the one-step approach and use the notation of Tesche et al. (2009).

5.1 One-step POLIPHON method

The procedure to separate dust and non-dust profiles of backscattering starts from the equation for the particle depolarization ratio

$$\delta_p = \frac{\beta_{nd}^\perp + \beta_d^\perp}{\beta_{nd}^\parallel + \beta_d^\parallel}. \quad (1)$$

β^\perp and β^\parallel are so-called cross- and parallel-polarized particle backscatter coefficients that can in principle be computed from the lidar return signals detected with the cross-polarized and parallel-polarized signal channels. The indices d and nd denote dust and non-dust aerosol components, respectively. The sum of all four backscatter contributions in Eq. (1) yields the particle backscatter coefficient β_p . The overall particle backscatter coefficient β_p is calculated in the way described in Sect. 2.1. For the sake of simplicity, the dependence on height z is not indicated.

As shown by Tesche et al. (2009), the particle depolarization ratio can be expressed by

$$\delta_p = \frac{\beta_{nd}\delta_{nd}(1 + \delta_d) + \beta_d\delta_d(1 + \delta_{nd})}{\beta_{nd}(1 + \delta_d) + \beta_d(1 + \delta_{nd})}, \quad (2)$$

with the dust and non-dust depolarization ratios $\delta_d = 0.31$ and $\delta_{nd} = 0.05$, respectively, as defined in Sect. 4.1. After substituting β_{nd} with $\beta_p - \beta_d$, we solve the resulting equation to obtain a solution for β_d (for $\delta_{nd} \leq \delta_p \leq \delta_d$),

$$\beta_d = \beta_p \frac{(\delta_p - \delta_{nd})(1 + \delta_d)}{(\delta_d - \delta_{nd})(1 + \delta_p)}. \quad (3)$$

The non-dust particle backscatter coefficient is defined as $\beta_{nd} = \beta_p - \beta_d$. For measured depolarization ratios $\delta_p < \delta_{nd}$,

we set $\beta_{nd} = \beta_p$. Depolarization ratios are frequently around 1–3% in boundary layers dominated by urban haze of marine particles. In these cases, the contribution by dust to the particle backscatter coefficient is negligible. For measured depolarization ratios $\delta_p > \delta_d$, we set $\beta_d = \beta_p$, i.e., in this case the non-dust aerosol contributions to the particle backscatter coefficient are negligible.

In the interpretation of the results of the one-step method, the dust or non-spherical particle fraction is assumed to contain only coarse-mode dust particles (Tesche et al., 2009; Ansmann et al., 2012). However, this dust fraction can also be interpreted as the total (fine + coarse) dust fraction. The obtained dust-related backscatter coefficients (β_d) may therefore be used to estimate the fine-mode dust backscatter coefficients ($0.3\beta_d$) by using an FMF dust fraction of 0.3, as discussed in Sect. 3. The resulting fine and coarse dust profiles (one-step method) can then be used for comparison with the respective backscatter profiles obtained with the two-step method as part of the uncertainty analysis (quality assurance checks).

5.2 Two-step POLIPHON method

In Fig. 5, the one-step and two-step methods are illustrated. In our two-step approach, we now introduce three types of aerosols: non-dust particles causing a particle linear depolarization ratio of $\delta_{nd} = 0.05$ or less, fine-mode dust causing a depolarization ratio of $\delta_{df} = 0.16$, and coarse-mode desert dust causing a particle depolarization ratio of $\delta_{dc} = 0.39$ (see Sect. 4.1).

Each of the two steps of the two-step method is similar to the one-step calculation (Eq. 3). In the first step, we separate the coarse-mode dust backscatter coefficient β_{dc} and the residual particle backscatter coefficient β_{nd+df} (caused by non-dust and fine-dust particles), and in the second round, we separate the non-dust backscatter coefficient β_{nd} from the fine-dust backscatter coefficient β_{df} .

The basic equation of our two-step retrieval scheme is

$$\delta_p = \frac{\beta_{nd}^\perp + \beta_{df}^\perp + \beta_{dc}^\perp}{\beta_{nd}^\parallel + \beta_{df}^\parallel + \beta_{dc}^\parallel}. \quad (4)$$

In the first step (see Fig. 5), we start from

$$\delta_p = \frac{\beta_{nd+df}^\perp + \beta_{dc}^\perp}{\beta_{nd+df}^\parallel + \beta_{dc}^\parallel}. \quad (5)$$

Analog to the step from Eq. (1) to (3), here we obtain for the coarse dust backscatter coefficient (within the depolarization range defined by $\delta_{nd+df,e} \leq \delta_p \leq \delta_{dc}$),

$$\beta_{dc} = \beta_p \frac{(\delta_p - \delta_{nd+df,e})(1 + \delta_{dc})}{(\delta_{dc} - \delta_{nd+df,e})(1 + \delta_p)}. \quad (6)$$

The residual particle backscatter coefficient is obtained from $\beta_{nd+df} = \beta_p - \beta_{dc}$. Analog to the one-step method, we need

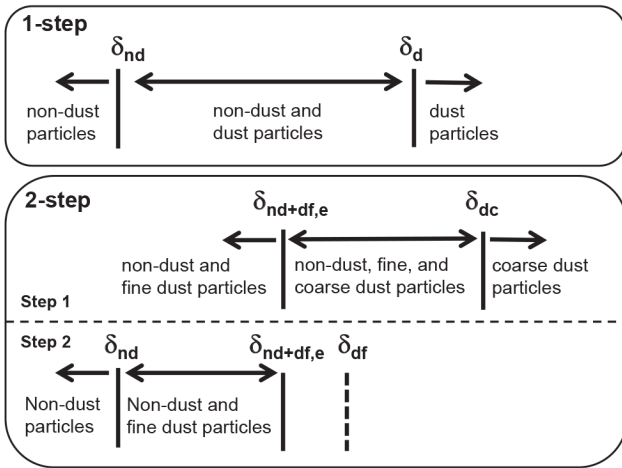


Figure 5. Illustration of the one-step and two-step POLIPHON methods to separate spherical particles from non-spherical dust particles (one-step method) and spherical particles, fine dust, and coarse dust particles (two-step method) by means of the particle depolarization ratio δ . In this paper, we use $\delta_{nd} = 0.05$ for non-dust (spherical) particles, $\delta_{nd+df,e} = 0.12$ for residual aerosol particles (after removing the coarse dust influence; see text for more details), $\delta_{df} = 0.16$ for fine dust, $\delta_d = 0.31$ for total dust, and $\delta_{dc} = 0.39$ for coarse dust.

to assume characteristic depolarization values for the upper boundary of the range of values (coarse dust, $\delta_{dc} = 0.39$) and the lower boundary $\delta_{nd+df,e}$, which describes the overall depolarization ratio for the residual aerosol (excluding the coarse dust fraction) and has to be estimated. Therefore we introduce index *e*. Analog to the one-step method, for measured depolarization ratios $\delta_p < \delta_{nd+df,e}$, we set the residual aerosol backscatter coefficient $\beta_{nd+df} = \beta_p$. In the case of $\delta_p > \delta_{dc}$, we set $\beta_{dc} = \beta_p$. Then, the aerosol contains coarse dust particles only.

The lower depolarization ratio boundary $\delta_{nd+df,e}$ can vary with location and height. So, first we need to estimate the contribution of non-dust particle backscatter to the residual aerosol backscatter coefficient β_{nd+df} for the lidar observation under study. In marine boundary layers, this fraction may be close to 100 % so that $\delta_{nd+df,e} = 0.05$. In the free troposphere, the spherical particle backscatter contribution may be close to zero in major dust outbreak plumes so that $\delta_{nd+df,e} = 0.16$. However, from the long-term AERONET and EARLINET observations at Cyprus we conclude that even in free-tropospheric dust plumes there is always a small amount of pollution aerosol (urban haze, biomass burning smoke). In the following derivations, in which we concentrate on lofted free-tropospheric dust containing plumes from Turkey and desert dust layers originating from Middle East deserts, we assume a non-dust particle backscatter contribution of 33 % to β_{nd+df} . 67 % of the backscatter coefficient β_{nd+df} is thus caused by fine-mode dust. Taking these non-dust and dust fine-mode fractions into consideration, we

obtain a depolarization ratio of $\delta_{nd+df,e} = 0.12$ with $\delta_{nd} = 0.05$ and $\delta_{df} = 0.16$. In principle, different $\delta_{nd+df,e}$ values for the PBL and free troposphere can be used or even a $\delta_{nd+df,e}(z)$ profile in the two-step derivations below. In the error analysis (Sect. 5.4), we checked the influence of uncertainties in $\delta_{nd+df,e}$ by computations with values of 0.08, 0.12, and 0.16 for this residual layer depolarization ratio.

The need for the estimate of the non-dust backscatter fraction results from the fact that we want to separate three aerosol components (spherical particles, fine dust, coarse dust) from depolarization ratio observations at a single wavelength of 532 nm. Single-wavelength polarization lidar observations allow us to separate two aerosol components only (Tesche et al., 2009). If we want to separate three aerosol components without introducing any assumption about the spherical particle fraction, we need polarization lidar measurements with a dual-wavelength polarization lidar operated for example at 532 and 1064 nm. Such lidar observations were performed during the SALTRACE campaigns at Barbados in 2013 and 2014, and the results of the two-step method will be presented in follow-up papers. Here, we concentrate on the two-step POLIPHON method for a single-wavelength 532 nm polarization lidar.

Before we can start the separation of non-dust (spherical) and fine-mode dust particles in the second round, we have to remove the optical effects of coarse-mode dust from the total particle backscatter coefficient and the particle depolarization ratio. The profile of the residual (non-dust and fine dust) backscatter coefficient is given by $\beta_{nd+df} = \beta_p - \beta_{dc}$, as stated above. Regarding the removal of the coarse-mode depolarization effect, one may use Eq. (11) of Tesche et al. (2009), here in the form of

$$\delta_{nd+df} = \frac{\beta_{dc}(\delta_p - \delta_{dc}) + \beta_{nd+df}\delta_p(1 + \delta_{dc})}{\beta_{dc}(\delta_{dc} - \delta_p) + \beta_{nd+df}(1 + \delta_{dc})}, \quad (7)$$

for the depolarization ratio range $\delta_p \leq \delta_{dc}$. However, it can be shown that the solving of Eq. (7) is equivalent to the simple setting according to

$$\delta_{nd+df} = \delta_p \quad \text{for} \quad \delta_p \leq \delta_{nd+df,e}, \quad (8)$$

$$\delta_{nd+df} = \delta_{nd+df,e} \quad \text{for} \quad \delta_p > \delta_{nd+df,e} \quad (9)$$

with our estimate $\delta_{nd+df,e} = 0.12$ for the Cyprus region. An example of the coarse-dust-corrected profiles of the particle backscatter coefficient and the depolarization ratio is shown in Sect. 6.

In the first round, we had to assume a characteristic value, $\delta_{nd+df,e}$, and now with Eqs. (8) and (9) we can check the quality of this estimate. If δ_{nd+df} is now clearly below 0.12 for most heights, one should repeat the full computation with a lower value for $\delta_{nd+df,e}$. If most δ_{nd+df} values are between 0.08 and 0.12 and thus close to $\delta_{nd+df,e} = 0.12$, then this estimate of 0.12 was sufficiently correct (and follow-up errors are below 20 %, as our simulations show).

In the second round, which is again similar to the one-step computations, we use $\delta_{\text{nd}} = 0.05$ and $\delta_{\text{df}} = 0.16$ (instead of $\delta_{\text{d}} = 0.31$ in the one-step approach, Sect. 5.1) as lower and upper depolarization limits in the separation of non-dust and fine-dust backscatter components. After the removal of the coarse-mode effects from the total particle depolarization ratio and the backscatter coefficient, the maximum value of the remaining depolarization profile ratio is now $\delta_{\text{nd+df}} = 0.12$, which corresponds to our assumption that the remaining part of the backscatter coefficient is caused by 33 % of non-dust particles and 67 % of fine-dust particles. Thus, by using $\delta_{\text{nd}} = 0.05$ and $\delta_{\text{df}} = 0.16$ as the lower and upper boundaries of the depolarization range, the fine-dust backscatter fraction is always $\leq 67\%$.

The second round starts from

$$\delta_{\text{nd+df}} = \frac{\beta_{\text{nd}}^{\perp} + \beta_{\text{df}}^{\perp}}{\beta_{\text{nd}}^{\parallel} + \beta_{\text{df}}^{\parallel}}. \quad (10)$$

Analog to the step from Eq. (5) to (6), now we obtain (for $\delta_{\text{nd+df}} \geq \delta_{\text{nd}}$)

$$\beta_{\text{df}} = \beta_{\text{nd+df}} \frac{(\delta_{\text{nd+df}} - \delta_{\text{nd}})(1 + \delta_{\text{df}})}{(\delta_{\text{df}} - \delta_{\text{nd}})(1 + \delta_{\text{nd+df}})} \quad (11)$$

with $\delta_{\text{nd}} = 0.05$ and $\delta_{\text{df}} = 0.16$ (see Fig. 5). The non-dust particle backscatter coefficient is given by $\beta_{\text{nd}} = \beta_{\text{nd+df}} - \beta_{\text{df}}$. Analog to the one-step method, for measured depolarization ratios $\delta_{\text{nd+df}} < \delta_{\text{nd}}$, we set the residual aerosol backscatter coefficient $\beta_{\text{nd}} = \beta_{\text{nd+df}}$.

By using characteristic lidar ratios S_{df} , S_{dc} , and S_{nd} in Table 1 (for the Cyprus area in this study), we convert the retrieved backscatter profiles β_{df} , β_{dc} , and β_{nd} into respective particle extinction coefficient profiles for the three resolved aerosol components. We set $S_{\text{df}} = S_{\text{dc}}$. It should be mentioned that lidar ratios for fine dust and coarse dust may also, in principle, differ considerably from each other, as the lidar ratio simulations of Gasteiger et al. (2011) indicate. Also in this respect, more laboratory and simulation studies are required.

In the final step of the two-step POLIPHON retrieval, the set of particle backscatter and extinction coefficients are converted into particle volume and mass concentrations. The mass concentrations M_{df} , M_{dc} , and M_{nd} for fine dust, coarse dust, and non-dust particles, respectively, can be obtained by using the following relationships (Ansmann et al., 2011a, 2012):

$$M_{\text{df}} = \rho_{\text{d}}(v_{\text{df}} / \tau_{\text{df}})\beta_{\text{df}}S_{\text{df}}, \quad (12)$$

$$M_{\text{dc}} = \rho_{\text{d}}(v_{\text{dc}} / \tau_{\text{dc}})\beta_{\text{dc}}S_{\text{dc}}, \quad (13)$$

$$M_{\text{nd}} = \rho_{\text{nd}}(v_{\text{nd}} / \tau_{\text{nd}})\beta_{\text{nd}}S_{\text{nd}}. \quad (14)$$

The particle densities, ρ_{d} and ρ_{nd} , are assumed to be 2.6 and 1.5 g cm⁻³, respectively (Ansmann et al., 2012). The conversion factors v_m / τ_m with column particle volume concentration v_m and corresponding optical thickness τ_m for aerosol component m are obtained from photometer observations as shown in Sect. 3. Here, we used the values given in Table 1.

5.3 Consistency check: POLIPHON vs. AERONET results

Because of the numerous assumptions and thus high degree of freedom in this two-step retrieval, we use AERONET observations as constraints to check the quality of the POLIPHON results. In other words, we checked to what extent our results and the assumptions made are consistent with the column-integrated values of fine- and coarse-mode optical properties as retrieved from the accompanying sun/sky photometer observations.

The AERONET parameters useful for comparison are the aerosol particle optical thickness AOT_{A} , the Ångström exponent AE_{A} (for the wavelength range around 500 nm, after AERONET from 440 to 870 nm), and the fine-mode fraction FMF_{A} after the O'Neill method (O'Neill et al., 2003a, b). These results are available with high temporal resolution, even for low 500 nm aerosol optical depths less than 0.1.

The respective lidar-derived quantities are AOT_{L} , AE_{L} , and FMF_{L} , which are calculated from the backscatter coefficient profiles in the planetary boundary layer (PBL), the free troposphere (FT), and using the parameters listed in Table 1. The PBL layer is simply defined here by aerosol concentration features. The PBL is defined as the layer that is directly affected by local aerosol sources (marine aerosol and urban pollution). We distinguish local PBL aerosol particles and FT particles after long-range transport.

We define the lidar-derived optical depth for a given aerosol type m (nd: $m = 1$; df: $m = 2$; dc: $m = 3$) and layer l (planetary boundary layer, PBL: $l = 1$; free troposphere, FT: $l = 2$) as follows:

$$\tau_{m,l} = S_{m,l} \int_{z_{l,\text{bot}}}^{z_{l,\text{top}}} \beta_{m,l}(z) dz. \quad (15)$$

Table 1 provides an overview of all input parameters. Lidar ratios for the PBL (the lowest 300–450 m of the troposphere) are found around 30 sr because of the marine influence, and around 60–80 sr in the FT from the CUT–AERONET long-term observations (2010–2014). More details on PBL- and FT-related lidar ratios can be found in Mamouri et al. (2013).

In Sect. 5, we compare solutions obtained with the one-step approach (nd: $m = 1$; d: $m = 2$; after Tesche et al., 2009) and the two-step method ($m = 1, 2$, and 3). Thus, we introduce the parameter N (number of aerosol components) with $N = 2$ in the case of the one-step method and $N = 3$ in the case of the two-step method. Now the total particle optical depth AOT_{L} derived from the lidar observations can be written as

$$\tau_{\text{L}} = \sum_{m=1}^N \sum_{l=1}^2 \tau_{m,l}. \quad (16)$$

Table 1. Overview of all input parameters used in our study. The particle lidar ratios S , and the PBL and FT Ångström exponents α for non-dust aerosol, are based on a careful analysis of the AERONET data in combination with the EARLINET data set for 2010–2014 with and without lofted aerosol layers in the FT over Limassol. We assume the same lidar ratio for fine and coarse dust. SAMUM-1 observations provided the dust Ångström exponents. The particle linear depolarization ratios δ are taken from the literature. Indices nd, df, dc, and d as used in the retrieval in Sect. 5 denote non-spherical particles, fine-mode dust, coarse-mode dust, and total (fine and coarse) dust, respectively. Particle extinction-to-volume conversion factors v/τ (see Sects. 3 and 5.2) are required to estimate mass and volume concentrations from the extinction coefficients.

Parameter	Symbol	Value	Source/reference
Lidar ratio (marine)		20 sr	Groß et al. (2011)
Lidar ratio (dust)	S_{df}, S_{dc}	35–40 sr	Mamouri et al. (2013)
Lidar ratio (urban haze, smoke)		50–70 sr	CUT, climatology
Lidar ratio (PBL, spherical)	$S_{nd}(\text{PBL})$	30 sr	CUT, climatology
Lidar ratio (FT, spherical)	$S_{nd}(\text{FT})$	60–80 sr	CUT, climatology
Ångström exponent (PBL, spherical)	$\alpha_{nd}(\text{PBL})$	0.5–1.5	CUT, climatology
Ångström exponent (FT, spherical)	$\alpha_{nd}(\text{FT})$	2.0	CUT, climatology
Ångström exponent (fine dust)	α_{df}	1.5	SAMUM-1, Fig. 3
Ångström exponent (coarse dust)	α_{dc}	−0.2	SAMUM-1, Fig. 3
Ångström exponent (total dust)	α_d	0.25	SAMUM-1, Fig. 3
Depolarization ratio (spherical)	δ_{nd}	0.05	Müller et al. (2007)
Depolarization ratio (fine dust)	δ_{df}	0.16	Sakai et al. (2010)
Depolarization ratio (coarse dust)	δ_{dc}	0.39	Sakai et al. (2010)
Depolarization ratio (total dust)	δ_d	0.31	Freudenthaler et al. (2009)
Conversion factor (spherical, FT)	v_{nd}/τ_{nd}	0.18×10^{-6} m	Ansmann et al. (2012)
Conversion factor (fine dust)	v_{df}/τ_{df}	0.3×10^{-6} m	Ansmann et al. (2012)
Conversion factor (coarse dust)	v_{dc}/τ_{dc}	0.9×10^{-6} m	Ansmann et al. (2012)

The lidar-derived column Ångström exponent AE_L is given by

$$\alpha_L = \frac{\sum_{m=1}^N \sum_{l=1}^2 \alpha_{m,l} \tau_{m,l}}{\sum_{m=1}^N \sum_{l=1}^2 \tau_{m,l}}, \quad (17)$$

with characteristic Ångström exponents in Table 1.

Typical Ångström exponents in Table 1 for the free-troposphere and boundary-layer aerosols over Cyprus are again obtained from the long-term AERONET–EARLINET studies (2010–2014). The pure dust Ångström exponents are from the SAMUM-1 campaign.

The fine-mode fraction FMF_L is computed from the lidar data as follows:

$$f_L = \frac{\sum_{m=1}^{N-1} \sum_{l=1}^2 \tau_{m,l}}{\sum_{m=1}^N \sum_{l=1}^2 \tau_{m,l}}. \quad (18)$$

5.4 Retrieval uncertainties

A detailed discussion of uncertainties in the backscatter coefficients for fine mode and coarse mode by means of the one-step method can be found in Tesche et al. (2009, 2011).

Errors in the retrieval of subsequent products such as extinction coefficients and mass concentrations are discussed by Ansmann et al. (2011a, 2012).

Uncertainties in the separation of the backscatter coefficients of spherical particles and fine and coarse dust particles are caused by four sources: (a) uncertainties in the computation of the basic products, i.e., of the particle depolarization ratios and backscatter coefficients as a function of signal noise and atmospheric input parameters, (b) uncertainties in the assumptions about characteristic depolarization ratios for fine dust and coarse dust, (c) uncertainties in the assumption about the non-dust particle backscatter contribution to the aerosol under study (first round of the two-step method), and (d) uncertainties in the input parameters in Table 1. According to the error discussions by Tesche et al. (2009) and Mamouri et al. (2013), the overall uncertainty in the basic particle backscatter coefficients is 5–10% in strong dust layers. In less pronounced aerosol layers, the uncertainty may increase to 20%. For well-detected desert dust layers (mixed with smoke), the uncertainty in dust-related and non-dust backscatter coefficients was found to be 15–20% (Tesche et al., 2009, 2011; Ansmann et al., 2012) (mainly caused by the uncertainty in the assumptions about the dust- and non-dust depolarization ratios) when using the one-step method. In less pronounced aerosol layers, the uncertainty may increase to 20–30%.

Further uncertainties of 10–20 % arise in the successive conversion of backscatter into extinction coefficients caused by the lidar ratio estimate, and in the mass concentration retrieval with uncertainties of 10–25 % in the dust mass density estimates, and 20–50 % in the used v/τ ratios, so that the overall uncertainty in the dust mass concentration values is 30–60 % when using the one-step POLIPHON approach.

These comparably low uncertainties allow us to use the dust and non-dust backscatter profiles of the one-step method to check the quality and reliability of the products obtained with the two-step method. Because of the larger number of input parameters, the uncertainties in the results of the two-step approach are much higher. The application of the error propagation theory is no longer possible, because we deal with input parameter errors much larger than 10–20 %. Many input parameters are simply not well enough known presently. We have to assume relative uncertainties in the fine-mode dust depolarization δ_{df} of about 50 % (δ_{df} from 0.1 to 0.22) and a similarly large uncertainty in the depolarization ratio δ_{nd+df} for the residual aerosol (δ_{nd+df} from 0.08 to 0.16). Our simulations for the same set of input parameters, except for a varying estimate of the fine-dust fraction (from 33 to 100 %) and corresponding variations of $\delta_{nd+df,e}$ from 0.08 to 0.16, lead to uncertainties within a factor of 2 in the fine-dust backscatter coefficients and about 10 % in the respective coarse-dust values in pronounced desert dust layers, when taking the computation with $\delta_{nd+df,e} = 0.12$ as the optimum solution. Simulations with characteristic fine-mode dust depolarization ratios δ_{df} of 0.1 and 0.22 (instead of the used 0.16) show that the relative errors of the fine-dust backscatter coefficients are comparably low, with values of 20–25 % in pronounced dust layers and less than 10 % in the respective coarse-dust backscatter values, so a wrong δ_{df} value does not affect the retrieval products much.

As a consequence of the partly large uncertainties, we use both, the one-step and two-step methods, in a complementary sense. As mentioned, the lower number of input parameters leads to lower uncertainties in the results of the one-step method. The two-step method, on the other hand, provides more insight into the dust optical properties. We use the dust backscatter profiles obtained with the one-step method as a quality standard. The sum of the fine and coarse dust backscatter profiles obtained with the two-step approach should approximately match the one obtained with the one-step method. As mentioned above, we may also assume a fine-mode dust contribution of about 30 % to backscatter, extinction, and optical depth (as the AERONET observations in Sect. 3 suggest) in the case of desert dust outbreaks. Then, we can roughly estimate the fine- and coarse-mode dust backscatter profiles from the total dust backscatter coefficient (one-step method) and compare these profiles with the respective ones obtained with the two-step method. Large discrepancies may then indicate that some basic assumption in the two-step data analysis must be changed and improved. The backscatter profile for the non-dust component obtained

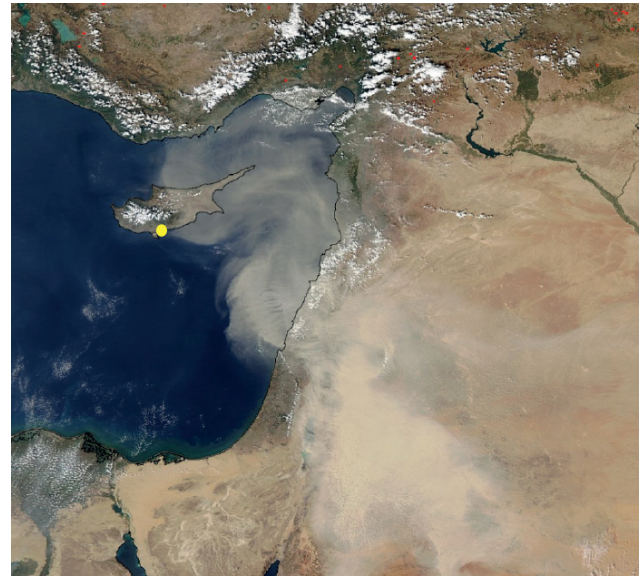


Figure 6. Dust outbreak from deserts in the Middle East reaching Cyprus on 28 September 2011 (TERRA–MODIS image, 08:30 UTC). Limassol is indicated by a yellow circle.

from the one-step retrieval should be close to the respective non-dust backscatter profile obtained with the two-step method. Furthermore, whenever AERONET sun/sky photometer observations are available, they should be used for further consistency checks in the way described in Sect. 5.3 and in the next Sect. 6.

6 Results: 26–30 September 2011 case study

6.1 Overview

The following case study serves as a test bed for the applicability of the new two-step POLIPHON method. Both the one-step and the two-step method are used to analyze a period with background fine soil dust from Turkey and desert dust from Syria. Layers of soil dust particles are frequently advected to Cyprus from areas of central and eastern Turkey and other arid regions further north of Turkey during the summer season (Nisantzi et al., 2014). These layers occur as lofted, vertically homogeneous plumes, mostly in the height range of 1–3 km a.s.l. As a unique feature, this background soil dust mainly consists of submicrometer particles, as the AE_A values indicate. A coarse-mode fraction is then not, or almost not, visible in the photometer observations. Episodically, desert dust outbreaks with a pronounced number concentration of supermicrometer particles from deserts in the Middle East and northern Africa reach Limassol and partly mix with this fine-mode soil dust from the north. Such an event is discussed in this section.

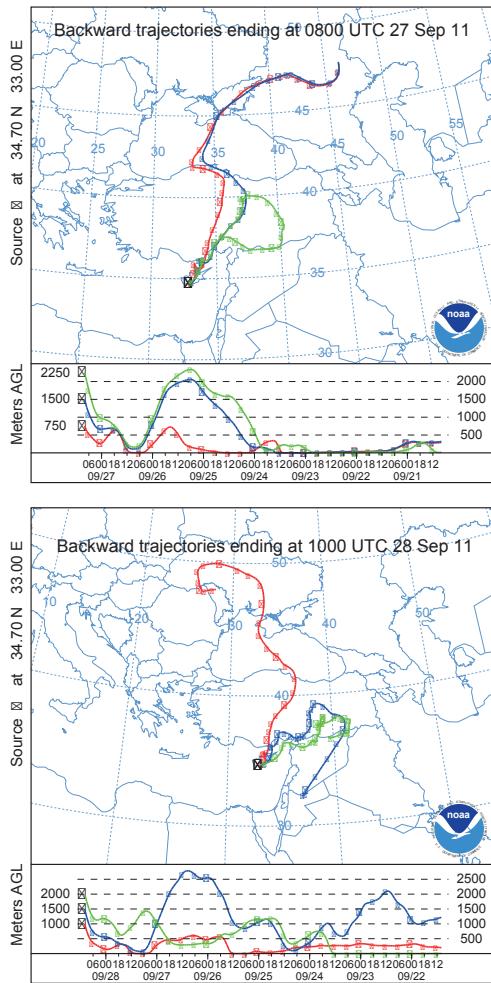


Figure 7. Seven-day backward trajectories arriving at Limassol, Cyprus, at different height levels (red, blue, green) on 27 September 2011, 08:00 UTC (top) and 28 September 2011, 10:00 UTC (bottom). Calculations are performed with the HYSPLIT (HYbrid Single-Particle Lagrangian Integrated Trajectory) model. Access via the NOAA ARL READY website (<http://www.arl.noaa.gov/HYSPLIT.php>).

Figure 6 shows the arrival of an extended desert dust layer over Limassol in the late morning of 28 September 2011. Before this, a northerly airflow from Turkey prevailed according to the backward trajectories in Fig. 7. The air mass transport changed from northerly advection on 26–27 September 2011 to more complex features in the regional aerosol transport resulting from a major Arabian dust outbreak on 28–29 September 2011.

The particle size distributions in Fig. 8 (taken from the AERONET database, level 2.0 data) show a bimodal shape, with a strong increase in the coarse-mode fraction when the dust outbreak arrived. The weak coarse mode on 26–27 September 2011 (blue lines in Fig. 8) consists most likely of marine particles, as Fig. 9 suggests. In this

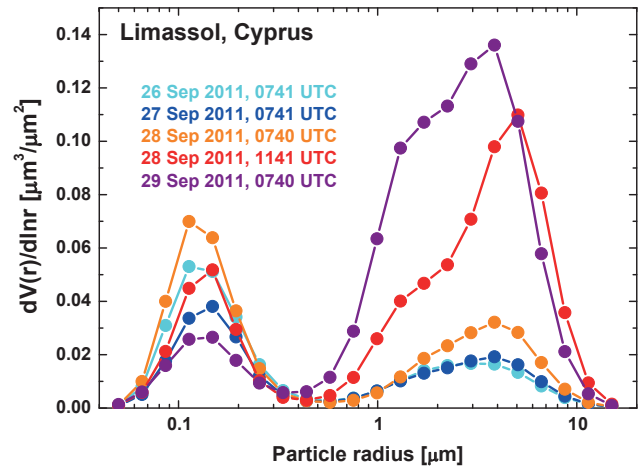


Figure 8. Column-integrated particle volume size distribution derived from AERONET sun/sky photometer observations at Limassol before (light blue and blue circles) and during the September 2011 dust outbreak (orange, red, and purple circles).

figure, pure marine size distributions as observed over Barbados with AERONET photometers during a field campaign (see the AERONET site of Barbados–SALTRACE, located on the western coast of Barbados, at the Caribbean Institute for Meteorology and Hydrology, CIMH, 13.1° N, 59.6° W, 110 m a.s.l.) and at Ragged Point (13.2° N, 59.4° W, 40 m a.s.l., eastern coast of Barbados) are compared with the observations over Limassol on 26–27 September 2011. As can be seen, the coarse modes over Limassol and Barbados are similar. Thus, the marine aerosol impact may fully explain the occurrence of the coarse mode in the volume size distributions of the Cyprus AERONET site on 26–27 September 2011. Marine particles are confined to heights of 300–450 m during the period studied here.

Typical marine AOTs are on the order of 0.04–0.06 at 500 nm, with a fine-mode contribution of 40–50%, as can be seen in Fig. 9 for the Barbados cases. If we subtract a potential fine-mode marine contribution of 0.025–0.03 and a similar PBL urban-haze contribution from the observed fine-mode AOT of 0.172, about 0.1–0.12 is left for the fine-mode aerosol in the free troposphere on 26–27 September 2011. The depolarization ratio profile in Fig. 10 shows that this fine-mode aerosol produces significantly enhanced depolarization ratios of around 10–15%. A considerable fraction of the free tropospheric fine-mode aerosol must therefore be dust. Since the aerosol crosses populated and industrialized areas in Turkey and further to the north, we must assume that a mixture of fine dust and other (spherical) aerosol components (urban haze, fire smoke) was present and lowered the overall particle depolarization ratio. As can be seen in Fig. 10, the depolarization ratio went up to almost 0.35 on 28 September 2011, when the Arabian dust arrived.

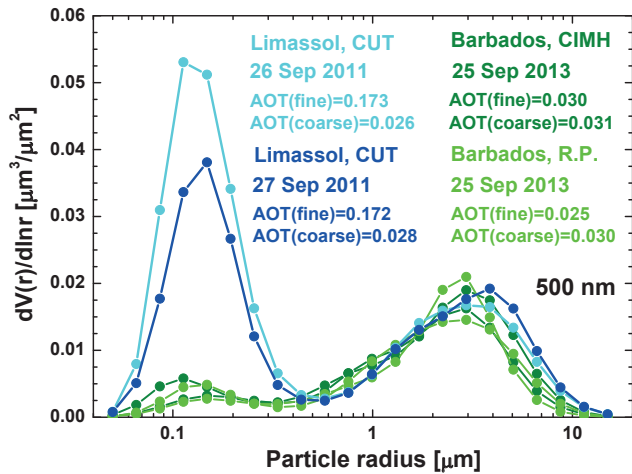


Figure 9. Column-integrated particle volume size distribution for pure marine conditions derived from AERONET observations at Barbados (CIMH and AERONET station Ragged Point, R.P.) on 25 September 2013 and for mixed aerosol conditions at the coastal AERONET station CUT, Limassol (measured at 07:41 UTC on 26 and 27 September 2011). The coarse mode at Limassol can be related to coarse marine particles. The pronounced fine mode is mostly related to urban haze in the boundary layer and fine-mode dust in the free troposphere.

An overview of the AERONET photometer observations from 26 to 30 September is presented in Fig. 11. The 500 nm AOT_A increased to values around 0.7 during the desert dust outbreak in the morning of 29 September 2011. At the same time, the 500 nm FMF_A dropped to values of 0.25. During the fine-mode dust days (26–27 September), FMF_A was high, with values greater than 0.9. Later on, the values from 0.4 to 0.7 indicated mixed aerosols. The Ångström exponent AE_A was around 1.8 during the fine-mode dust days, and dropped to values of 0.5–1.0 when the major dust outbreak dominated the aerosol conditions over Limassol. The minimum value of $AE_A = 0.25$ was observed in the early morning of 29 September 2011.

6.2 Retrieval of fine-mode and coarse-mode backscatter coefficients

Figures 12–15 show examples of applications of the extended POLIPHON method. Input parameters such as the characteristic particle depolarization ratios for non-dust, fine, and coarse dust are taken from Table 1. As outlined in Sect. 5.2, it is assumed that roughly 33 % of the residual (total minus coarse dust) particle backscatter is caused by anthropogenic aerosol (urban haze and biomass burning smoke). In this first feasibility study on the potential of polarization lidar to provide detailed insight into fine-mode and coarse-mode dust optical and microphysical properties, we avoid presenting error bars to keep the figures simple and to facilitate the discussion.

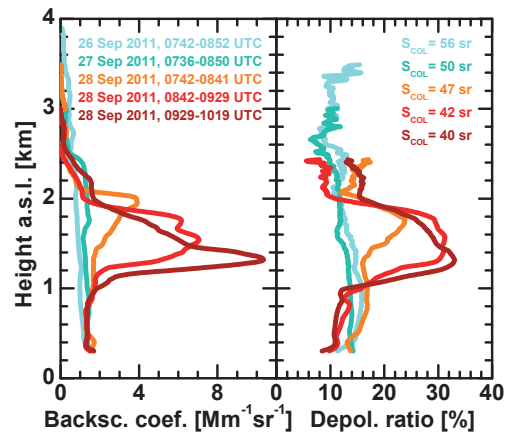


Figure 10. 532 nm particle backscatter coefficient (left) and particle linear depolarization ratio (right) in the free troposphere during a northerly airflow with fine-mode dust (26–27 September 2011) and during the arrival of a strong Arabian dust outbreak on the morning of 28 September 2011. The column lidar ratios S_{col} for the entire vertical aerosol column are derived from combined photometer–lidar data analysis (Mamouri et al., 2013). 60–70 min of lidar return signals are averaged.

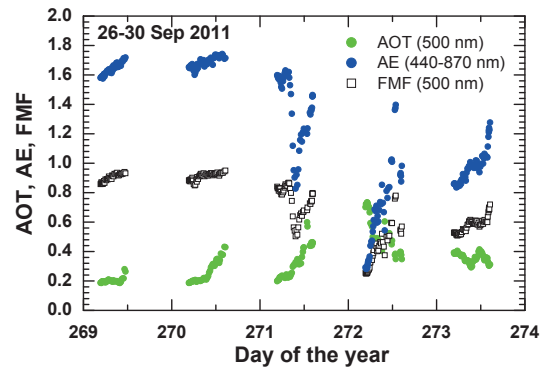


Figure 11. AERONET observations of 500 nm aerosol particle optical thickness (AOT), Ångström exponent (AE), and fine-mode fraction (FMF) for the 26–30 September 2011 period.

The aerosol conditions as observed before the arrival of the major dust storm are given in Fig. 12. Such aerosol conditions caused by an air mass transport from Turkey with a mixture of fire smoke and soil dust motivated us to develop the two-step method. As can be seen, the free tropospheric aerosol layer extended from about 350 to 3500 m in height. The particle depolarization ratio ranges from 0.1 to 0.14 in the main aerosol layer up to 2500 m. The slightly enhanced depolarization ratio values in the boundary layer (< 300 m) are probably caused by road dust and surface near local dust transport from arid regions of Cyprus. The colored numbers in Fig. 12 are the lidar-derived AOT_L values (after Eq. 15) for the different aerosol components. In addition, the lidar-derived Ångström exponent AE_L (Eq. 17) and

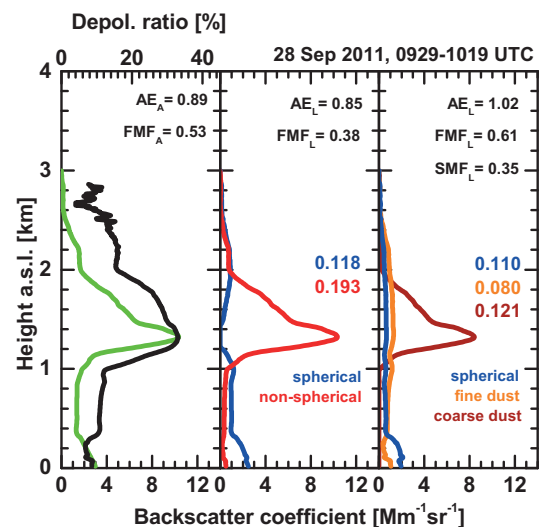
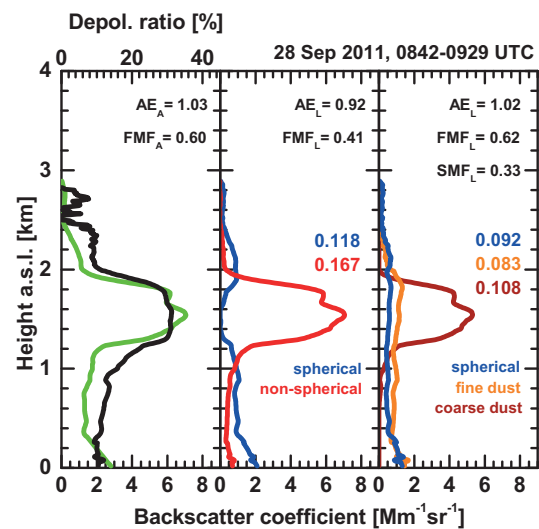
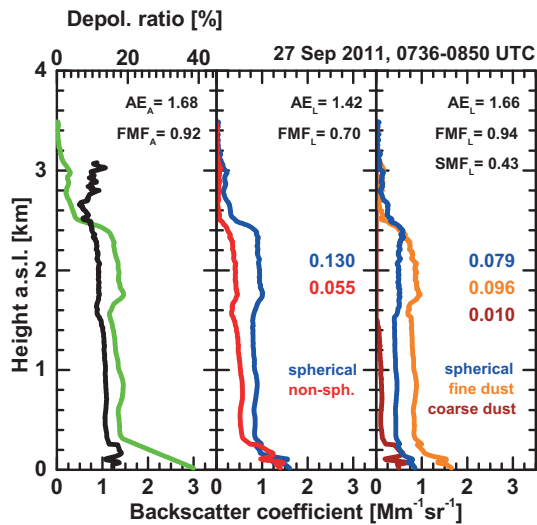


Figure 12. (Left) 532 nm particle backscatter coefficient (green) and particle linear depolarization ratio (black), (center) particle backscatter coefficient for non-spherical and spherical particles (one-step method), and (right) particle backscatter coefficient for spherical particles, fine and coarse dust (two-step method) observed on 29 September 2011, 07:36–08:50 UTC. 74 min of lidar return signals are thus averaged. The corresponding AOTs for the different aerosol components are given as colored numbers, computed from the backscatter profiles multiplied by appropriate lidar ratios as given in Table 1. AE, FMF, and SMF denote Ångström exponent, fine-mode fraction, and spherical mode fraction (ratio of spherical particle AOT to total AOT), respectively. Index A indicates AERONET values, index L lidar-derived results obtained by means of Eqs. (17) and (18). In the central panel, $FMF_L = SMF_L$. For the lowest 300 m a linear increase of the total backscatter coefficient from 300 m height to the surface (see left panel) is assumed.

fine-mode fraction FMF_L (Eq. 18) are presented and compared with the respective AERONET values (FMF_A , AE_A) given in the left panels of the figures. All the quantities are computed by using the aerosol parameters in Table 1.

In the case of FMF_L for the one-step method, we assume that all dust particles (non-spherical particles) belong to the coarse mode and that all spherical particles belong to the fine mode. We used the total dust AE value of 0.25 in Table 1 in the computation of the respective AE_L value (one-step method).

The AERONET Ångström exponent was high, and indicated the absence of a pronounced coarse dust mode. During such events, the comparison of the one-step and two-step results is not possible. The sum of the fine and coarse dust backscatter profiles does not match the one for the dust backscatter coefficient after the one-step method. Consequently, the non-dust profiles obtained with the one-step and two-step methods do not match, either. The main reason is that a coarse mode is missing, and the application of a characteristic desert dust depolarization ratio $\delta_d = 0.31$ is not an appropriate input parameter in the one-step method under

Figure 13. Same as Fig. 12, except for two periods on (top) 28 September 2011, 08:42–09:29 UTC (47 min signal average) and (bottom) 28 September 2011, 09:29–10:19 UTC (50 min signal average).

these conditions. Similar one-step and two-step dust profiles are obtained when a dust depolarization ratio of 0.16 is used in the one-step data analysis.

As can be seen in Fig. 12, the one-step method leads to a comparably large coarse-mode particle backscatter fraction for depolarization ratios of 0.1–0.14. Accordingly, FMF_L is much lower with 0.70 at these specific background fine-mode dust conditions than the AERONET value of $FMF_A = 0.92$. As a consequence, a significant disagreement is also found in terms of the Ångström exponent ($AE_A = 1.68$, $AE_L = 1.42$). A much better agreement is obtained when using the two-step method. The fine-mode fraction now consists of spherical particles and fine-mode dust. This leads to an increase in the FMF_L and AE_L values. The good agreement of the results of the two-step method with the AERONET results may

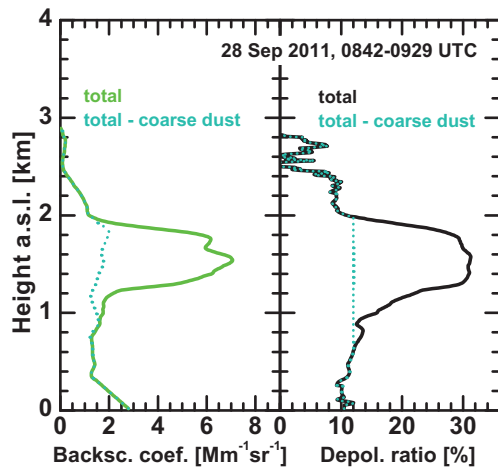


Figure 14. Total particle backscatter coefficient (green, left), the particle linear depolarization ratio (black, right) and the respective residual aerosol (spherical particles and fine dust) contributions (blue dotted, obtained after step 1 of the two-step data analysis). The backscatter and depolarization ratio profiles for the residual aerosol are used as input for step 2 in the two-step approach (see Fig. 5).

be interpreted as an indication that the used fine-mode dust depolarization ratio $\delta_{df} = 0.16$ is appropriate.

Figure 13 shows the aerosol conditions after the arrival of desert dust. A pronounced dust layer was found between 1 and 2 km in height, and high depolarization ratios of greater than 0.3 were observed in this layer, indicating a strong contribution of coarse dust particles to light backscattering (see Fig. 10). The AERONET values of AE_A and FMF_A significantly decreased compared to the values observed the day before (Fig. 11). Both the applications of the one-step and the two-step methods reveal large coarse-dust-related backscatter coefficients between 1 and 2 km in height and a mixture of fine-mode and coarse-mode particles below and above the main desert dust layer. According to the solutions of the two-step approach in the right panels of Fig. 13, a considerable part of the fine-mode backscatter coefficient is caused by dust. By resolving fine and coarse dust with the two-step method again, a better agreement of the AERONET- and lidar-derived AE and FMF values is obtained.

Now the results of the one-step and two-step POLIPHON solutions can be compared in the way suggested in Sect. 5.4. The main conclusions of this comparison are as follows: (a) the sum of the fine and coarse dust backscatter profiles (two-step method) match approximately the respective one-step dust backscatter profile. (b) Assuming roughly a fine dust fraction of 0.3, we find good agreement between the resulting one-step fine and coarse dust profiles and the respective two-step solutions for most parts of the profiles. (c) To obtain an idea about the uncertainties, the one-step and two-step computations show the range of possible coarse dust backscatter values. We can never exclude the possibility that coarse-mode dust is present, as indicated by the one-step

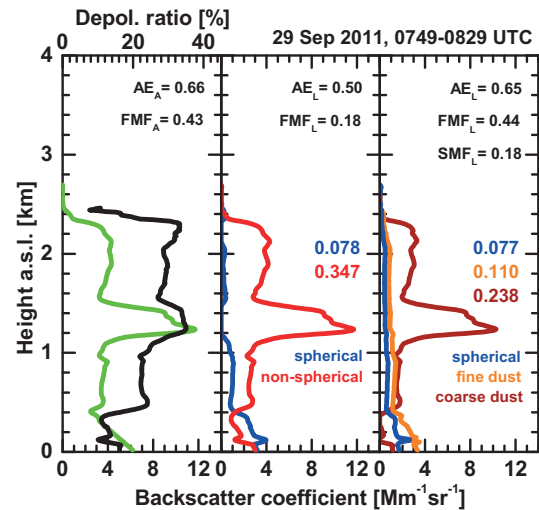


Figure 15. Same as Fig. 12, except for a morning measurement on 29 September 2011, 07:49–08:29 UTC (40 min signal average).

results. The two-step profiles at heights less than 1.2 km suggest the absence of such coarse dust.

Figure 14 provides more insight into the two-step data analysis. The figure shows the same case as presented in Fig. 13 (top panels). By using the depolarization limits of 0.12 and 0.39, we determine the backscatter contributions of the residual aerosol particles and coarse dust particles (see Fig. 5, the first step of the two-step method). Before we can apply the second step, we have to remove the coarse dust impact on the backscatter coefficient ($\beta_{nd+df} = \beta_p - \beta_{dc}$) and on the particle depolarization ratio by means of Eqs. (8) and (9). These resulting coarse-dust-corrected backscatter and depolarization ratio profiles are shown in Fig. 14 as blue dotted lines. They are the input profiles for the second round of the two-step method.

Figure 15 shows the dust outbreak situation on 29 September 2011, when the desert dust plume influenced the entire tropospheric column up to 2.5 km in height and covered large parts of the eastern Mediterranean. At all heights above the PBL up to 2.5 km, the particle depolarization ratio was higher than 0.2. The 500 nm AOT was close to 0.43, with a strong coarse dust contribution of 0.235 (two-step method). Both the one-step and the two-step methods reveal a total dust AOT of close to 0.35. Again, the two-step method results (AE_L , FMF_L) are in better agreement with the AERONET products (AE_A , FMF_A) than the values obtained with the one-step approach. The one-step method yields a rather low fine-mode fraction of 0.18 which is equal to the spherical mode fraction ($SMF_L = 0.18$) in the case of the two-step method.

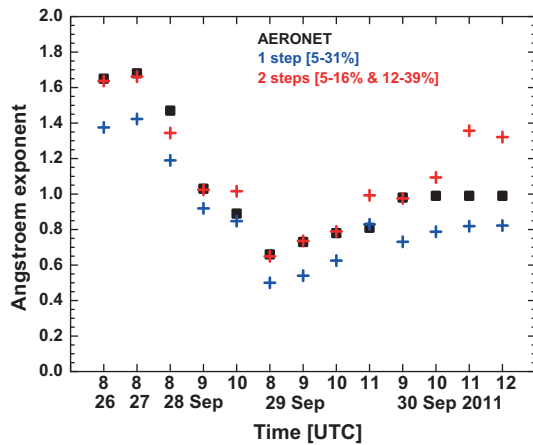


Figure 16. Comparison of Ångström exponents (AE_A vs. AE_L) derived from AERONET observations (black squares) and retrieved from the lidar measurements (blue crosses, one-step method, red crosses, two-step method) for the entire measurement period from 26 to 30 September 2011.

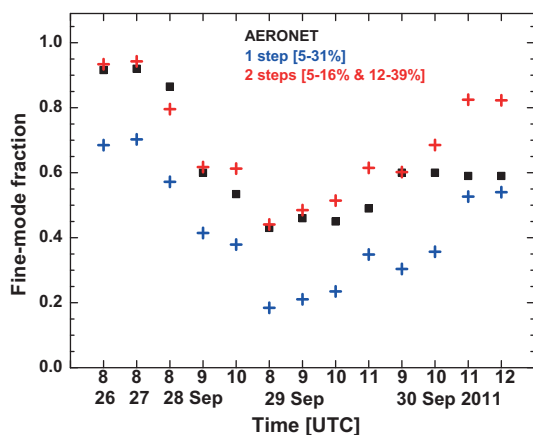


Figure 17. Same as Fig. 16, except for the fine-mode fraction (FMF_A vs. FMF_L).

6.3 Consistency check with the AERONET results

Figures 16 and 17 provide an overview of the AERONET- and lidar-derived AE and FMF values for the entire observational period from 26 to 30 September 2011. The AE_L values depend on many assumptions regarding the spectral dependence of backscattering and the extinction of a variety of aerosol types (according to Table 1). Therefore, the comparison with the AE_A values may only provide hints of the quality of the AE_L values. The FMF values, on the other hand, are not largely influenced by assumptions, so that the good agreement between FMF_A and FMF_L (the two-step method) is a clear sign that our two-step approach worked successfully. Especially for the 26–29 September period, a very good agreement between the AERONET values and the lidar data is obtained. At the end of our observational

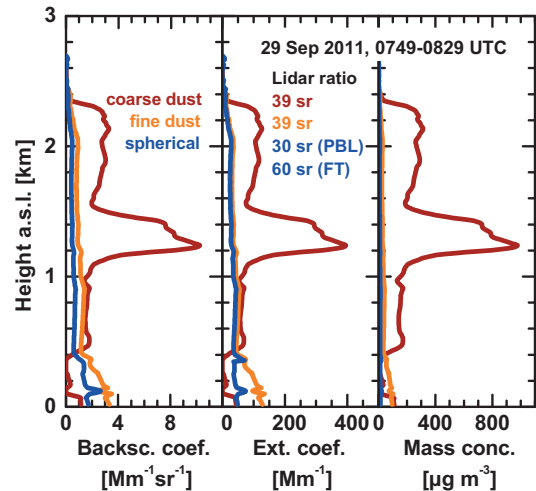


Figure 18. 532 nm particle backscatter and extinction coefficients, and particle mass concentrations computed from the backscatter coefficients in Fig. 15 by means of the two-step method, the lidar-ratio information in Table 1, and volume-to-extinction conversion factors as discussed in Sect. 3 and given in Table 1.

period (30 September 2011), when the backward trajectories (not presented) showed a complex air mass transport structure with prevailing westerly winds, both methods are no longer in good agreement with the AERONET results. The main reason is that the selected assumption of $\delta_{nd+df,e} = 0.12$ was no longer appropriate at lower heights (below 1.5 km in height), where the impact of marine aerosol increased significantly. At these conditions, $\delta_{nd+df,e} = 0.08$ would be more appropriate.

6.4 Particle extinction and mass concentration profiles

For completeness, we briefly present further products of the extended POLIPHON method. Figure 18 provides an example of the computation of the particle extinction coefficients and mass concentrations from the particle backscatter coefficients after Eqs. (12)–(14), for each aerosol component (fine spherical, fine dust, coarse dust). The results for the lowermost 300 m have to be interpreted with caution, because all profiles rely on the assumption of a linear increase in the backscatter coefficient from 300 m towards the ground. The uncertainties in the extinction coefficients and mass concentrations in the free troposphere are estimated to be on the order of 25–40 % and around 50 %, respectively.

As can be seen in Fig. 18, fine-mode dust significantly contributes to the total particle extinction coefficient in the free troposphere as demonstrated in Sect. 3. Extinction values for fine-mode dust are on the order of 30–50 Mm^{-1} .

The mass concentration profiles show that coarse dust mostly contributes to particle mass in the free troposphere. Maximum values of close to 1000 $\mu g m^{-3}$ are found at 1.2 km height. Fine dust mass concentrations are around 40 $\mu g m^{-3}$

in the free troposphere and $50\text{--}100\ \mu\text{g m}^{-3}$ close to the ground. The fine spherical particles show far fewer mass concentrations of $15\text{--}20\ \mu\text{g m}^{-3}$ in the PBL and $10\text{--}15\ \mu\text{g m}^{-3}$ in the free troposphere. Thus, fine dust can dominate $\text{PM}_{1.0}$ levels at the ground during dust outbreak situations.

7 Conclusions

The height-resolved separation of the optical properties of fine and coarse dust by means of the polarization lidar technique has been proposed for the first time. The well-established one-step POLIPHON method to separate dust and non-dust particle optical properties has been extended. Now, fine-mode and coarse-mode dust profiles in terms of particle backscatter and extinction coefficients, volume and mass concentrations can be derived after introducing the two-step data analysis scheme. The one-step and two-step methods together deliver a complementary data set indicating the range of potential solutions for the three separated aerosol components. The overall data set indicates the uncertainties in the obtained profiles. A feasibility study based on complex aerosol observations with EARLINET lidar and AERONET sun/sky photometer observations over Limassol, Cyprus, demonstrated the applicability and usefulness of the extended POLIPHON method. Such a step forward in the application of polarization lidar techniques provides important new insight into dust properties for atmospheric and environmental research.

The new retrieval technique requires a considerable number of assumptions. In the next step, multiwavelength polarization lidars, providing depolarization ratios at two wavelengths (Sugimoto and Lee, 2006; Groß et al., 2011; Kanitz et al., 2014) or even three wavelengths (Ansmann et al., 2014; Müller et al., 2014), with additional Raman or high-spectral-resolution channels for extinction and backscattering profiling, are the best candidates for an almost unambiguous separation of fine and coarse dust profiles. Three-wavelength polarization lidar observations in pure Saharan dust plumes and mixed plumes of Saharan dust, marine particles, and even biomass burning smoke, performed at Barbados in the framework of SALTRACE, are now available to develop a multiwavelength polarization lidar version of the extended POLIPHON method.

Future laboratory studies of dust optical properties as observed with lidar, in the way performed by Sakai et al. (2010), should be extended to cover laser wavelengths of 355, 532, and 1064 nm, and should be conducted separately for fine-mode and coarse-mode dust. In addition, we need further simulation studies, as suggested by Gasteiger et al. (2011) for the mentioned laser wavelengths. First attempts have already been undertaken (J. Gasteiger, personal communication, 2014). These efforts should focus on the particle linear depolarization ratio and the lidar ratio, and this separately for irregularly shaped fine dust and coarse dust.

Acknowledgements. We are grateful to AERONET for high-quality sun/sky photometer measurements in Cyprus, Morocco, and Barbados. We thank Joseph Prospero and his team of Miami University for taking care of the Ragged Point AERONET observations, and the SAMUM and SALTRACE teams for taking care of the SAMUM and SALTRACE photometer observations. The authors thank the CUT Remote Sensing Laboratory, especially Argyro Nisantzi, for their support. We gratefully acknowledge the NOAA Air Resources Laboratory (ARL) for the provision of the HYSPLIT transport and dispersion model and/or the READY website (<http://www.ready.noaa.gov>) used in this publication.

Edited by: G. Pappalardo

References

- Ångström, A.: The parameters of atmospheric turbidity, *Tellus*, 16, 64–75, 1964.
- Ansmann, A., Bösenberg, J., Chaikovsky, A., Comerón, A., Eckhardt, S., Eixmann, R., Freudenthaler, V., Ginoux, P., Komguem, L., Linné, H., López Márquez, M. A., Matthias, V., Mattis, I., Mitev, V., Müller, D., Music, S., Nickovic, S., Pelon, J., Sauvage, L., Sobolewsky, P., Srivastava, M. K., Stohl, A., Torres, O., Vaughan, G., Wandinger, U., and Wiegner, M.: Long-range transport of Saharan dust to northern Europe: the 11–16 October 2001 outbreak observed with EARLINET, *J. Geophys. Res.*, 108, 4783, doi:10.1029/2003JD003757, 2003.
- Ansmann, A., Tesche, M., Groß, S., Freudenthaler, V., Seifert, P., Hiebsch, A., Schmidt, J., Wandinger, U., Mattis, I., Müller, D., and Wiegner, M.: The 16 April 2010 major volcanic ash plume over central Europe: EARLINET lidar and AERONET photometer observations at Leipzig and Munich, Germany, *Geophys. Res. Lett.*, 37, L13810, doi:10.1029/2010GL043809, 2010.
- Ansmann, A., Tesche, M., Seifert, P., Groß, S., Freudenthaler, V., Apituley, A., Wilson, K. M., Serikov, I., Linné, H., Heinold, B., Hiebsch, A., Schnell, F., Schmidt, J., Mattis, I., Wandinger, U., and Wiegner, M.: Ash and fine-mode particle mass profiles from EARLINET-AERONET observations over central Europe after the eruptions of the Eyjafjallajökull volcano in 2010, *J. Geophys. Res.*, 116, D00U02, doi:10.1029/2010JD015567, 2011a.
- Ansmann, A., Petzold, A., Kandler, K., Tegen, I., Wendisch, M., Müller, D., Weinzierl, B., Müller, T., and Heintzenberg, J.: Saharan mineral dust experiments SAMUM-1 and SAMUM-2: What have we learned?, *Tellus B*, 63, 403–429, doi:10.1111/j.1600-0889.2011.00555.x, 2011b.
- Ansmann, A., Seifert, P., Tesche, M., and Wandinger, U.: Profiling of fine and coarse particle mass: case studies of Saharan dust and Eyjafjallajökull/Grimsvötn volcanic plumes, *Atmos. Chem. Phys.*, 12, 9399–9415, doi:10.5194/acp-12-9399-2012, 2012.
- Ansmann, A., Althausen, D., Kanitz, T., Engelmann, R., Skupin, A., Baars, H., Klepel, A., Haarig, M., Heinold, B., Tegen, I., Toledano, C., Prescod, D., and Farrell, D.: Saharan dust long-range transport: SALTRACE lidar observations at Barbados and aboard RV Meteor (Guadeloupe to Cape Verde) versus dust transport modelling, *Proceedings, DUST 2014 – International Conference on Atmospheric Dust, Castellana Marina, Italy, 1–6 June 2014*, 2014.
- Baars, H., Ansmann, A., Althausen, D., Engelmann, R., Artaxo, P., Pauliquevis, T., and Souza, R.: Further evidence for significant

- smoke transport from Africa to Amazonia, *Geophys. Res. Lett.*, 38, L20802, doi:10.1029/2011GL049200, 2011.
- Barnaba, F. and Gobbi, G. P.: Aerosol seasonal variability over the Mediterranean region and relative impact of maritime, continental and Saharan dust particles over the basin from MODIS data in the year 2001, *Atmos. Chem. Phys.*, 4, 2367–2391, doi:10.5194/acp-4-2367-2004, 2004.
- Burton, S. P., Vaughan, M. A., Ferrare, R. A., and Hostetler, C. A.: Separating mixtures of aerosol types in airborne High Spectral Resolution Lidar data, *Atmos. Meas. Tech.*, 7, 419–436, doi:10.5194/amt-7-419-2014, 2014.
- Chaikovskiy, A., Dubovik, O., Goloub, P., Tanré, D., Pappalardo, G., Wandinger, U., Chaikovskaja, L., Denisov, S., Grudo, Y., Lopatsin, A., Karol, Y., Lapyonok, T., Korol, M., Osipenko, F., Savitsky, D., Slesar, A., Apituley, A., Alados-Arboledas, L., Biniotoglou, I., Comerón, A., Granados-Muñoz, M. J., Papayannis, A., Perrone, M. R., Pietruczuk, A., De Tomasi, F., Wagner, J., and Wang, X.: Algorithm and software for the retrieval of vertical aerosol properties using combined lidar/radiometer data: dissemination in EARLINET network, *Proceedings, 26th International Laser Radar Conference, Porto Heli, Greece*, 399–402, 2012.
- Chen, W.-N., Tsai, F.-J., Chou, C. C.-K., Chang, S.-Y., Chen, Y.-W., and Chen, J.-P.: Optical properties of Asian dusts in the free atmosphere measured by Raman lidar at Taipei, Taiwan, *Atmos. Environ.*, 41, 7698–7714, 2007.
- Chew, B. N., Campbell, J. R., Reid, J. S., Giles, D. M., Welton, E. J., Salinas, S. V., and Liew, S. C.: Tropical cirrus cloud contamination in sun photometer data, *Atmos. Environ.*, 45, 6724–6731, doi:10.1016/j.atmosenv.2011.08.017, 2012.
- Dahlkötter, F., Gysel, M., Sauer, D., Minikin, A., Baumann, R., Seifert, P., Ansmann, A., Fromm, M., Voigt, C., and Weinzierl, B.: The Pagami Creek smoke plume after long-range transport to the upper troposphere over Europe – aerosol properties and black carbon mixing state, *Atmos. Chem. Phys.*, 14, 6111–6137, doi:10.5194/acp-14-6111-2014, 2014.
- DeMott, P. J., Prenni, A. J., Liu, X., Kreidenweis, S. M., Peters, M. D., Twohy, C. H., Richardson, M. S., Eidhammer, T., and Rogers, D. C.: Predicting global atmospheric ice nuclei distributions and their impacts on climate, *P. Natl. Acad. Sci. USA*, 107, 11217–11222, doi:10.1073/pnas.0910818107, 2010.
- Dubovik, O., Sinyuk, A., Lapyonok, T., Holben, B., Mishchenko, M., Yang, P., Eck, T., Volten, H., Muñoz, O., Veihelmann, B., van der Zande, W. J., Leon, J. F., Sorokin, M., and Slutsker, I.: Application of spheroid models to account for aerosol particle non-sphericity in remote sensing of desert dust, *J. Geophys. Res.*, 111, D11208, doi:10.1029/2005JD006619, 2006.
- Fiebig, M., Petzold, A., Wandinger, U., Wendisch, W., Kiemle, C., Stifter, A., Ebert, M., Rother, T., and Leiterer, U.: Method, accuracy, and inferable properties applied to a biomass-burning aerosol and its radiative forcing, *J. Geophys. Res.*, 107, 8130, doi:10.1029/2000JD000192, 2002.
- Freudenthaler, V., Esselborn, M., Wiegner, M., Heese, B., Tesche, M., Ansmann, A., Müller, D., Althausen, D., Wirth, M., Fix, A., Ehret, G., Knippertz, P., Toledano, C., Gasteiger, J., Garhammer, M., and Seefeldner, M.: Depolarization ratio profiling at several wavelengths in pure Saharan dust during SAMUM 2006, *Tellus B*, 61, 165–179, doi:10.1111/j.1600-0889.2008.00396.x, 2009.
- Gasteiger, J., Wiegner, M., Groß, S., Freudenthaler, V., Toledano, C., Tesche, M., and Kandler, K.: Modelling lidar-relevant optical properties of complex mineral dust aerosols, *Tellus B*, 63, 725–741, doi:10.1111/j.1600-0889.2011.00559.x, 2011.
- Groß, S., Tesche, M., Freudenthaler, V., Toledano, C., Wiegner, M., Ansmann, A., Althausen, D., and Seefeldner, M.: Characterization of Saharan dust, marine aerosols and mixtures of biomass-burning aerosols and dust by means of multi-wavelength depolarization and Raman lidar measurements during SAMUM 2, *Tellus B*, 63, 706–724, doi:10.1111/j.1600-0889.2011.00556.x, 2011.
- Groß, S., Freudenthaler, V., Wiegner, M., Gasteiger, J., Geiß, A., and Schnell, F.: Dual-wavelength linear depolarization ratio of volcanic aerosols: Lidar measurements of the Eyjafjallajökull plume over Maisach, Germany, *Atmos. Environ.*, 48, 85–96, 2012.
- Groß, S., Esselborn, M., Weinzierl, B., Wirth, M., Fix, A., and Petzold, A.: Aerosol classification by airborne high spectral resolution lidar observations, *Atmos. Chem. Phys.*, 13, 2487–2505, doi:10.5194/acp-13-2487-2013, 2013.
- Heese, B. and Wiegner, M.: Vertical aerosol profiles from Raman polarization lidar observations during the dry season AMMA field campaign, *J. Geophys. Res.*, 113, D00C11, doi:10.1029/2007JD009487, 2008.
- Heintzenberg, J.: The SAMUM-1 experiment over Southern Morocco: overview and introduction, *Tellus B*, 61, 2–11, 2009.
- Holben, B. N., Eck, T. F., Slutsker, I., Tanré, D., Buis, J. P., Setzer, A., Vermote, E., Reagan, J. A., Kaufman, Y. J., Nakajima, T., Lavenu, F., Jankowiak, I., and Smirnov, A.: AERONET – a federated instrument network and data archive for aerosol characterization, *Remote Sens. Environ.*, 66, 1–16, 1998.
- Kanitz, T., Engelmann, R., Heinold, B., Baars, H., Skupin, A., and Ansmann, A.: Tracking the Saharan air layer with shipborne lidar across the tropical Atlantic, *Geophys. Res. Lett.*, 41, 4762–4766, doi:10.1002/2013GL058780, 2014.
- Kok, J. F.: A scaling theory for the size distribution of emitted dust aerosols suggests climate models underestimate the size of the global dust cycle, *P. Natl. Acad. Sci. USA*, 108, 1016–1021, doi:10.1073/pnas.1014798108, 2011.
- Lopatín, A., Dubovik, O., Chaikovskiy, A., Goloub, P., Lapyonok, T., Tanré, D., and Litvinov, P.: Enhancement of aerosol characterization using synergy of lidar and sun-photometer coincident observations: the GARRLiC algorithm, *Atmos. Meas. Tech.*, 6, 2065–2088, doi:10.5194/amt-6-2065-2013, 2013.
- Mahowald, N., Albani, S., Kok, J. F., Engelstaeder, S., Scanza, R., Ward, D. S., and Flanner, M. G.: The size distribution of desert dust aerosols and its impact on the Earth system, *Aeolin Research*, 15, 53–71, doi:10.1016/j.aeolia.2013.09.002, 2014.
- Mamouri, R. E., Ansmann, A., Nisantzi, A., Kokkalis, P., Schwarz, A., and Hadjimitsis, D.: Low Arabian extinction-to-backscatter ratio, *Geophys. Res. Lett.*, 40, 4762–4766, doi:10.1029/2013grl.50898, 2013.
- Müller, D., Mattis, I., Wandinger, U., Ansmann, A., Althausen, A., and Stohl, A.: Raman lidar observations of aged Siberian and Canadian forest fire smoke in the free troposphere over Germany in 2003: microphysical particle characterization, *J. Geophys. Res.*, 110, D17201, doi:10.1029/2004JD005756, 2005.
- Müller, D., Ansmann, A., Mattis, I., Tesche, M., Wandinger, U., Althausen, D., and Pisani, G.: Aerosol-type-dependent lidar ra-

- tios observed with Raman lidar, *J. Geophys. Res.*, 112, D16202, doi:10.1029/2006JD008292, 2007.
- Müller, D., Weinzierl, B., Petzold, A., Kandler, K., Ansmann, A., Müller, T., Tesche, M., Freudenthaler, V., Esselborn, M., Heese, B., Althausen, D., Schladitz, A., Otto, S., and Knippertz, P.: Mineral dust observed with AERONET Sun photometer, Raman lidar, and in situ instruments during SAMUM 2006: Shape-independent particle properties, *J. Geophys. Res.*, 115, D07202, doi:10.1029/2009JD012520, 2010.
- Müller, D., Hostetler, C. A., Ferrare, R. A., Burton, S. P., Chernyakin, E., Kolgotin, A., Hair, J. W., Cook, A. L., Harper, D. B., Rogers, R. R., Hare, R. W., Cleckner, C. S., Obland, M. D., Tomlinson, J., Berg, L. K., and Schmid, B.: Airborne Multiwavelength High Spectral Resolution Lidar (HSRL-2) observations during TCAP 2012: vertical profiles of optical and microphysical properties of a smoke/urban haze plume over the northeastern coast of the US, *Atmos. Meas. Tech.*, 7, 3487–3496, doi:10.5194/amt-7-3487-2014, 2014.
- Murayama, T., Okamoto, H., Kaneyasu, N., Kamataki, H., and Miura, K.: Application of lidar depolarization measurement in the atmospheric boundary layer: effects of dust and sea-salt particles, *J. Geophys. Res.*, 104, 31781–31792, doi:10.1029/1999JD900503, 1999.
- Murayama, T., Müller, D., Wada, K., Shimizu, A., Sekiguchi, M., and Tsukamoto, T.: Characterization of Asian dust and Siberian smoke with multiwavelength Raman lidar over Tokyo, Japan in spring 2003, *Geophys. Res. Lett.*, 31, L23103, doi:10.1029/2004GL021105, 2004.
- Nabat, P., Solmon, F., Mallet, M., Kok, J. F., and Somot, S.: Dust emission size distribution impact on aerosol budget and radiative forcing over the Mediterranean region: a regional climate model approach, *Atmos. Chem. Phys.*, 12, 10545–10567, doi:10.5194/acp-12-10545-2012, 2012.
- Nisantzi, A., Mamouri, R. E., Ansmann, A., and Hadjimitsis, D.: Injection of mineral dust into the free troposphere during fire events observed with polarization lidar at Limassol, Cyprus, *Atmos. Chem. Phys. Discuss.*, 14, 17299–17329, doi:10.5194/acpd-14-17299-2014, 2014.
- Nishizawa, T., Okamoto, H., Sugimoto, N., Matsui, I., Shimizu, A., and Aoki, K.: An algorithm that retrieves aerosol properties from dual-wavelength polarized lidar measurements, *J. Geophys. Res.*, 112, D06212, doi:10.1029/2006JD007435, 2007.
- Noh, Y. M., Müller, D., Lee, H. L., and Choi, T. J.: Influence of biogenic pollen on optical properties of atmospheric aerosols observed by lidar over Gwangju, South Korea, *Atmos. Environ.*, 69, 139–147, doi:10.1016/j.atmosenv.2012.12.018, 2013.
- O'Neill, N. T., Dubovik, O., and Eck, T. F.: Modified Ångström exponent for the characterization of submicrometer aerosols, *Appl. Optics*, 40, 2368–2375, 2003a.
- O'Neill, N. T., Eck, T. F., Smirnov, A., Holben, B. N., and Thulasiraman, S.: Spectral discrimination of coarse and fine mode optical depth, *J. Geophys. Res.*, 108, 4559, doi:10.1029/2002JD002975, 2003b.
- Papayannis, A., Amiridis, V., Mona, L., Tsaknakis, G., Balis, D., Bösenberg, J., Chaikovski, A., De Tomasi, F., Grigorov, I., Mattis, I., Mitev, V., Müller, D., Nickovic, S., Pérez, C., Pietruczuk, A., Pisani, G., Ravetta, F., Rizi, V., Sicard, M., Trickl, T., Wiegner, M., Gerding, M., Mamouri, R. E., D'Amico, G., and Pappalardo, G.: Systematic lidar observations of Saharan dust over Europe in the frame of EARLINET (2000–2002), *J. Geophys. Res.*, 113, D10204, doi:10.1029/2007JD009028, 2008.
- Sakai, T., Nagai, T., Zaizen, Y., and Mano, Y.: Backscattering linear depolarization ratio measurements of mineral, sea-salt, and ammonium sulfate particles simulated in a laboratory chamber, *Appl. Optics*, 49, 4441–4449, 2010.
- Sasano, Y., Browell, E. V., and Ismail, S.: Error caused by using a constant extinction/backscattering ratio in the lidar solution, *Appl. Optics*, 24, 3929–3932, 1985.
- Shimizu, A., Sugimoto, N., Matsui, I., Arai, K., Uno, I., Murayama, T., Kagawa, N., Aoki, K., Uchiyama, A., and Yamazaki, A.: Continuous observations of Asian dust and other aerosols by polarization lidars in China and Japan during ACE-Asia, *J. Geophys. Res.*, 109, D19S17, doi:10.1029/2002JD003253, 2004.
- Sugimoto, N. and Lee, C. H.: Characteristics of dust aerosols inferred from lidar depolarization measurements at two wavelengths, *Appl. Optics*, 45, 7468–7474, 2006.
- Sugimoto, N., Uno, I., Nishikawa, M., Shimizu, A., Matsui, I., Dong, X., Chen, Y., and Quan, H.: Record heavy Asian dust in Beijing in 2002: Observations and model analysis of recent events, *Geophys. Res. Lett.*, 30, 1640, doi:10.1029/2002GL016349, 2003.
- Tesche, M., Ansmann, A., Müller, D., Althausen, D., Engelmann, R., Freudenthaler, V., and Groß, S.: Vertically resolved separation of dust and smoke over Cape Verde using multiwavelength Raman and polarization lidars during Saharan Mineral Dust Experiment 2008, *J. Geophys. Res.*, 114, D13202, doi:10.1029/2009JD011862, 2009.
- Tesche, M., Müller, D., Groß, S., Ansmann, A., Althausen, D., Freudenthaler, V., Weinzierl, B., Veira, A., and Petzold, A.: Optical and microphysical properties of smoke over Cape Verde inferred from multiwavelength lidar measurements, *Tellus B*, 63, 677–694, doi:10.1111/j.1600-0889.2011.00549.x, 2011.
- Wandinger, U. and Ansmann, A.: Experimental determination of the lidar overlap profile with Raman lidar, *Appl. Optics*, 41, 511–514, 2002.
- Wagner, J., Ansmann, A., Wandinger, U., Seifert, P., Schwarz, A., Tesche, M., Chaikovsky, A., and Dubovik, O.: Evaluation of the Lidar/Radiometer Inversion Code (LIRIC) to determine microphysical properties of volcanic and desert dust, *Atmos. Meas. Tech.*, 6, 1707–1724, doi:10.5194/amt-6-1707-2013, 2013.
- Zhang, L., Kok, J. F., Henze, D. K., Li, Q., and Zhao, C.: Improving simulations of fine dust surface concentrations over the western United States by optimizing the particle size distribution, *Geophys. Res. Lett.*, 40, 3270–3275, doi:10.1002/grl.50591, 2013.